Study of the Seismic Behavior of the "Old Municipal Chambers" Building in Christchurch, New Zealand

Rui Marques [a]*, João M. Pereira [a], Paulo B. Lourenço [a], Will Parker [b], Masako Uno [b]

[a] ISISE, Department of Civil Engineering, University of Minho, Guimarães, Portugal

[b] Opus International Consultants Limited, Christchurch, New Zealand

* Address correspondence to Rui Marques, Department of Civil Engineering, University of Minho, Campus de Azurém, Guimarães, 4800-058, Portugal; E-mail: marquesmnc@sapo.pt

Abstract: This paper presents a study of the seismic behavior of the "Old Municipal Chambers" building in Christchurch, which was damaged by earthquakes in 2010 and 2011. In view of its seismic vulnerability and retrofitting, finite element and equivalent frame models were used for pushover analysis. Predictions allow identifying the weak parts of the building and its expected failure modes, which are in agreement with the observed damage. Computations seem however conservative, because the building capacity curves provide insufficient strength to survive the registered earthquakes. By considering the floors as bidirectional diaphragms in the simplified model, a better behavior is observed.

Keywords: Cultural Heritage Buildings; Seismic Assessment; Micro-Macro Element Models; Pushover Analysis; Seismic Retrofit

Short Title: Seismic Behavior of the "Old Municipal Chambers" Building

1. Introduction

Since early times, buildings have been an essential support to civilization, which still are important material and cultural legacies for a country. These buildings are often termed ancient, historic or monumental. Masonry buildings constructed in the last 150 years are often called “traditional”, which is a term that possibly better expresses the more earthly cultural and societal reasons that inspired their construction. In many cases, these buildings have not received the same attention given to more ancient buildings. Still, these buildings are an inspiration to our life style and have relevance for the Tourism sector.

Earthquakes are one of the main causes of human losses in the built heritage, particularly for traditional buildings, because these are commonly used for lodging or public offices. Traditional buildings are also interesting case studies, since they include often early engineered anti-seismic constructive techniques. The evaluation of the efficiency of these techniques in seismic events is an important reference for the current practice of construction and retrofitting of buildings.

Early seismic design of traditional buildings was mainly based on empirical rules. Only later, in the beginning of the 20th century, the request to consider a given horizontal acceleration arose. After 1950s the concept of ductility was introduced in codes, even if in a rather simple way. By the beginning of the 21th century, in the sequence of extensive experimental and analytical studies, and as a response to several destructive earthquakes, new codes were introduced (e.g., European code CEN 2004, Italian code NTC 2008, New Zealand code NZS 2004, North American code ATC 2005), which present methodologies to specifically consider the inelastic capacity of buildings through performance-based procedures.

Given the evolution of seismic design, traditional buildings are potentially vulnerable to seismic events. This work presents the particular case of a building in New Zealand

constructed in 1880s and made of unreinforced brick masonry. In this country around 3600 unreinforced masonry buildings were constructed between 1870 and 1950 presenting a collective financial value (in 2009) of approximately NZ$1.5 billion [Russell and Ingham, 2010]. A huge number of buildings of this kind were constructed around the world. According to Russell *et al.* [2007] the New Zealand's unreinforced masonry buildings constructed in this period present low similarity in their construction details and material properties to structures in other seismic-prone areas, particularly in Europe and Asia. However, all masonry buildings incorporate the same basic principle of earthquake resistance: an assembly of walls supporting floors at given levels providing a dissipative response to the whole structure, for which a similar seismic assessment procedure can be applied.

Masonry is a complex material to model due to the inherent anisotropy and variability of properties. Only a few authors implemented constitutive non-linear models able to consider different strength and deformation capacity along the material axes, e.g. Lourenço [2000] and Calderini and Lagomarsino [2008] for finite elements, Milani *et al.* [2007] for limit analysis and Peña *et al.* [2007] for rigid block analysis. These models are not widely disseminated and can be hard to apply to traditional buildings given the difficulties to characterize the existing fabric with a high level of detail. An alternative, lowest-complexity level, solution is to adopt simple geometrical indices, e.g. Lourenço and Roque [2006], to make a first, non-binding, screening of seismic assessment. The present work addresses the capability of modern advanced tools widely disseminated, based on pushover analysis, for the seismic assessment of traditional unreinforced masonry buildings through a complex and earthquake damaged case study. For this purpose, a finite element model combined with a standard isotropic smeared cracking approach and a simplified equivalent frame model will be compared and discussed in detail.

2. Description of the Studied Building

The “Old Municipal Chambers” in Figure 1 is a Category I heritage building in New Zealand, which was designed in 1886 by architect Samuel Hurst Seager in the Queen Anne style. The building was opened in 1887, functioning originally as the Municipal Chambers of the Christchurch City Council. After different usages as Government and Commerce offices, since 2002 the building was opened as “Our City O-Tautahi”, a community center used for civic facilities and recreation.

The two storey building is constructed in solid brick (mainly red) and presents wooden floors. Drawings of the building are shown in Figures 2 and 3, as structural plans and representative elevations of the building. The building dimensions are about 19.5 × 19.5 m^2 with external walls having a thickness of 0.47 m and 0.36 m in the ground storey and first storey, respectively. The storey heights are about 4.5 m and 3.2 m, respectively for the ground floor and first floor elevation. A second storey is constructed under the roof level at 11.9 m. Finally, the “Council Chamber” and the SE turret have a roof height of 14.6 m. The building is likely to have deep foundations made in concrete and extending down to a gravel layer.

The building was subjected to subsequent modifications, which will be detailed in a next section. Photographic details of the building are shown in Figure 4, namely one of the two main statues “Industry” and “Concord” in the South wall of the Council Chamber, a bottom-to-top view of window’s frames in the West elevation, and an inspected zone in the support of the ground floor. Good quality of the brick masonry works is evident.

2.1. Effects of the 2010 and 2011 Christchurch Earthquakes

Christchurch has historically registered several quakes, namely in 1888 with a magnitude Mw of 7.0-7.3 and an epicenter 100 km North-West of the city, and in 1901 with

an Mw of 6.9 and epicenter in Cheviot. Recently, the city was subjected to two strong quakes, the first in September 2010 with a M_w of 7.1 and epicenter 40 km West of the city, and the second in February 2011 with a M_w of 6.3 and epicenter only 10 km South-East of the city. Since the 2010 earthquake many aftershocks have been registered and the response spectra for the main events are given in Figure 5, which were obtained from Bradley [2011]. These were recorded in the "Christchurch Hospital" Station near the studied building.

The studied building seems not to have been much affected by the 1888 and 1931 Christchurch earthquakes, but due to the recent 2010-2011 earthquakes the building is significantly damaged. The building, included in the city layout as shown in Figure 6a was closed and the surrounding areas were made restricted for people, with shoring and barriers, e.g. in Figure 6b, generating a significant impact in the local access and panorama. The interior of the building currently can only be visited by photos, as shown in Figure 7 for the Council Chamber.

Based on a photographic survey, a mapping of the damage identified on the building façades was made. The North façade presents the crack pattern in Figure 8, with diffused stepped diagonal and vertical cracks appearing on the eastern and western upper ends of the wall, respectively. In the East façade, presented in Figure 9, the gable on the northern end of the wall has collapsed due to out-of-plane overturning. The masonry work at the left of this gable is severely damaged, with partial loss of the tile covering.

The western end of the South façade presents several diagonal cracks around the openings and the Industry statue niche, as shown in Figure 10. The West wall, adjacent to the Council Chamber, suffered severe damage on the northern and southern upper ends as well as in the connection between the chimney and the outer wall (Figure 11). Note the clear failure of the spandrel at the right of Figure 11, due to combined in-plane and out-of-plane motions.

The building has been strongly shored on the external walls, and particular care was made to protect the South façade as can be observed in Figure 6b. A detailed description of the shoring works is reported by Walters and Parker [2011]. There was no information regarding the damage in the internal walls of the building, because access inside the building was denied due to safety reasons. Given that the September 2010 and February 2011 earthquakes have different epicenter locations in the fault system, the main shakings of the two events probably occurred in different directions. However, accounting for the significant in-plane damage observed in North and South façades, it seems that the building was mainly subjected to shaking in direction E-W. However, the differentiation of damage due to the two earthquakes is not objective as the photographic survey available refers mainly to the period after the February 2011 earthquake.

Regarding the February 2011 earthquake, the short duration of the seismic event is noted, for which the most severe shaking lasted only twelve seconds. In the case of unreinforced masonry and brittle collapse due e.g. to overturning, the event duration can have an important influence in the building damage and response. However, this effect cannot be directly accounted with pushover analysis, requiring a time history analysis or, most likely, a probabilistic approach.

3. Seismic Analysis

The present study focuses on the seismic assessment of the Old Municipal Chambers building. The simulation model is based on drawings, pictures and in situ observation, and considers the original structure of the building. The subsequent modifications to the original drawings were only incorporated in the simplified analytical model, given the simplicity of the changes and the low running time of the analyses. The strategy defined for the seismic assessment is based on a comparative analysis of the results obtained from two different

modeling approaches easily available for engineering applications, based on a general purpose finite element method (FEM) software and a masonry tailored equivalent frame (simplified) method (EFM) software.

The FEM model was built in the DIANA software [TNO, 2009], adopting a total strain crack model based on the direct implementation of the experimental observations [Selby and Vecchio, 1993]. Like the traditional smeared crack models, see e.g. Rots [1998], the total strain based crack models follow a smeared approach for the fracture energy, but provide a more robust numerical algorithm. The software and the constitutive model have been used to model complex masonry buildings, e.g. by Ramos and Lourenço [1994], Lourenço *et al.* [2007] or Lignola and Cosenza [2009]. EFM models are becoming widely available for engineering practice, mostly based on the Italian experience, see Marques and Lourenço [2011]. Here, the EFM model was idealized using the TreMuri computer code [Galasco *et al.*, 2009]. Again, applications to the structural analysis of complex masonry buildings can be found, e.g. in Galasco *et al.* [2004] and Fusco *et al.* [2008].

3.1. Assumptions

The lower ends of the walls at the ground floor are considered fixed to the ground (0.0 m level), which is in agreement with the existing deep foundations for the building. The ground floor was considered leveled at 0.0 m. A dead load of 2 kN/m^2 was considered to simulate the weight of the timber floors, while live loads of 0.9 kN/m^2 and 0.6 kN/m^2, respectively for the first and second floors, which were based on code specifications for quasi-permanent loading, due to the scarce information about the existing live loads in the building. It is noted that the value of the live load considered amounts only to about 5% of the total mass, having almost no influence in the seismic response. The roof was not modeled to reduce the complexity of the FEM model, being replaced by linear loads, namely vertical

loads of 5 kN/m on the longer walls of the Council Chamber, of 4 kN/m on the turret walls and of 3 kN/m on the remaining walls supporting the roof.

The floors are one-way timber joists with wood planks. The wood is assumed with a weight of 6.5 kN/m^3 and an elastic modulus of 12,000 MPa. The floors are assumed to be made with wooden beams of section 0.15 × 0.3 m^2 spaced of 0.5 m. The floors are considered spanning along the smallest dimension of each room. In the case of the FEM the floors were modeled as a distribution of concentrated masses along the edges of the supporting walls. Note that this modeling approach is conservative, as it is neglecting the connection and diaphragm effects of the floors, known to be important to the seismic response of the building, particularly concerning the prevention of out-of-plane mechanisms.

The properties for the masonry are presented in Table 1 and were derived from experimental local data in Christchurch, the Italian Code NTC 2008 and the recommendations given in Lourenço [2009]. Note that, for example, for masonry compressive strength a formula similar to $K\ f_b^{0.7}\ f_m^{0.3}$ from Eurocode 6 [CEN, 2004] has been proposed for New Zealand by Lumantarna [2012], based on the adjustment of extensive experimental data. The fracture energy values are obtained as follows: the tensile value is obtained from the few tests available in the literature [van der Pluijm, 1999]; the compressive value is obtained from a ductility factor of 1.6 mm, equal to the ratio between the fracture energy and the ultimate strength [Lourenço, 2009]. Note that a stone lintel was added to the windows in the external walls.

3.2. Procedure

The definition of the geometric model was based on a CAD drawing, used for both models. The nonlinear static (pushover) analysis was selected for evaluation of the seismic response of the building. The analysis is made using an incremental-iterative procedure,

which allows to predict the base shear-displacement response (capacity curve) and to simulate the damage evolution in the individual elements. The structure is in a first stage submitted to the vertical loading, and then the analysis proceeds with horizontal loading replicating the seismic load, for which a mass-proportional pattern is assumed, as recommend in Lourenço *et al.* [2011] for the analysis of masonry structures without box behavior.

The pushover analysis is often linked to displacement-based seismic assessment, using a methodology such as the N2 method [Fajfar and Fischinger, 1988], where the expected displacement demands in design earthquakes are computed by means of a response spectrum analysis of an equivalent single degree-of-freedom system. Afterwards, these displacements are compared with the displacement capacities at given performance levels. In the present study, pushover analysis is used, through the prediction of deformation and damage, to identify the weak features of the structure and to design the strengthening that will be implemented in the building.

It is noted that out-of-plane mechanisms can lead to extensive damage on buildings with weak (or no) box behavior, i.e. with insufficient connections between walls and between walls and diaphragms. The prevention of these collapse mechanisms is possibly the most important action in seismic retrofitting actions, as the global seismic response of a building can only be exploited if early out-of-plane damage is avoided. In this work, the assessment of out-of-plane mechanisms is not directly made for the EFM model, where critical zones are only identified based on global pushover analyses and local mechanisms must be prevented by improving connections, but it is made in the FEM model, where out-of-plane mechanisms are possible.

3.2.1. FEM model

In the FEM model, the walls were simulated as shell elements and the columns were simulated as beam elements. The analytical model was discretized in several parts creating a mesh (Figure 12). This mesh was automatically generated by DIANA, and then manipulated and controlled in order to obtain a good quality mesh. The walls are discretized with quadrilateral 8 nodes shell elements (CQ40S) shown in Figure 13a, with 2 × 2 Gauss integration in plane and 7-point Simpson integration through thickness. This curved shell element is based on isoparametric degenerated-solid approach by introducing two shell hypotheses: normals remain straight, but not necessarily normal to the reference surface. Transverse shear deformation is included according to the Mindlin-Reissner theory; the normal stress component in the normal direction of a lamina basis is forced to zero.

The columns are discretized with 3 nodes beam elements (CL18B), using 2 Gauss integration points along the bar axis and 7 × 7 Simpson integration in the cross section. The element follows the Mindlin-Reissner theory, taking shear deformation into account, and are based on an isoparametric formulation that assumes displacements and rotations of the beam axis normals are independent and are respectively interpolated from the nodal displacements and rotations. The final mesh has 56,106 nodes and 17,940 elements. Because the floors were modeled as a distribution of concentrated masses, 3,567 elements of concentrated mass points (PT3T) were also created. The total mass of the model is 918.5 tonnes.

The nonlinear behavior of the masonry is modeled through the adoption of a total strain crack model [TNO, 2009], as addressed before. The stress-strain diagrams follow an exponential relationship to simulate tensile inelastic behavior and a parabolic relationship to simulate compressive inelastic behavior (Figure 13b). The procedure for the pushover analysis uses the regular Newton-Raphson method with an energy convergence criterion with a tolerance of 10^{-3}.

3.2.2. EFM model

In the case of the EFM, modeling of the building has been made using a macro-element approach idealized by Gambarotta and Lagomarsino [1996]. The adopted macro-element, presented in Figure 14, has 8 d.o.f. and reproduces the two main in-plane failure mechanisms of masonry: a) bending-rocking by a mono-lateral elastic contact between the edge interfaces and b) shear-sliding by considering a uniform shear deformation distribution on the central part of the element.

For the case of the bending-rocking mechanism, the panel strength is computed assuming a rectangular stress block for the masonry in compression, through the formula given in Figure 15a. Regarding the shear mechanism, a shear-stepped mode is normally assumed for solid brick masonry, e.g. by the Mann and Müller criterion [1982], should it be fully solid and adequately bonded (which is likely not the case for thick walls in New Zealand). Furthermore, the authors have obtained in the past over-conservative responses when considering the Mann and Müller criterion for shear-sliding. For this reason, the Turnšek and Čačovič [1970] criterion was adopted, which is also the specified shear failure criterion in the Italian code for existing masonry buildings, even for shear-stepped mode.

Thus, the shear failure is assumed to occur by diagonal tension cracking when the principal tensile stress at the centroid of the panel reaches the masonry tensile strength, according to the Turnšek and Čačovič [1970] criterion in Figure 15b. In both cases of bending-rocking and shear machanisms, an elastic–perfectly plastic (bilinear) law is assumed with limited ductility, as originally proposed by Tomaževič [1978], which is an approximation to the envelope of lateral cyclic loading tests on masonry panels. The ductility is limited by ultimate drifts defined for the masonry panels based on experimental evidence, namely Anthoine *et al.* [1995].

Modeling is based on the discretization of the walls in macro-elements, which are representative of pier-panels and lintels contiguous to the openings (Figure 16a). The connection between piers and lintels is made through rigid nodes, which remain typically undamaged during seismic action. 3D nodes with 5 d.o.f. are used to connect transversal walls, as shown in Figure 16b. The walls are the bearing elements, while floors, apart from providing vertical loading to the walls, are considered as plane stiffening elements (orthotropic 3 or 4 nodes membrane elements). The local flexural behavior of the floors and the out-of-plane response of the walls are not computed because they are considered negligible with respect to the global building response, which is governed by their in-plane behavior.

The geometric model and an automatic mesh were first generated in the 3Muri commercial version [S.T.A. DATA, 2010]. Then, the mesh was enhanced by using the TreMuri research version, namely to model the arches and gables [Galasco *et al.*, 2009]. The final 3D macro-element model is shown in Figure 17, where a plan with the numbering of the walls and the floor model is also presented. Figure 18 presents the detailed macro-element model, for two views of the building. The model includes about 500 elements among piers, lintels, elastic beams, wood beams and stone lintels, and 250 connection nodes. The total mass of the model is 912.7 tonnes (0.6% difference from the FEM model).

The window arches in the ground storey were modeled as elastic beams with large axial and flexural stiffness, in order to simulate their low deformability. The two arched gables were modeled as a set of macro-elements, as shown in Figure 19 for the gable in the East façade. In this case, the lateral zones of the main arch were modeled as two rigid bodies connected by the masonry lintel E34. The top gable was modeled through piers with increasing heights approaching the inclined shape. In each side, piers are rigidly connected creating a kind of a large spandrel body around 3D nodes N7 and N11. The lateral bodies are

connected by a masonry lintel supported on a rigid beam simulating the small arch. The described modeling approach for the East gable intends mainly to simulate the stiffness contribution and weight distribution through the involved 3D nodes to the global structure. The results based on damage identification, presented below, demonstrate the adequacy of the adopted modeling approach. It is noted that in this case out-of-plane mechanisms are not considered.

4. Analytical Results

The results obtained in the analyses are now presented, for the FEM and EFM models, and also for the original and modified building structures. Four analyses are always carried out, covering the two main directions of the building with positive and negative loading signs. The results presented next include the predicted damage in the structural elements, the deformed shape of the building and the capacity curves.

4.1. Results Corresponding to the Original Design

First, results from the pushover analyses applied to models in correspondence with the original building drawings by Samuel Seager in 1886 are shown, for the FEM and EFM models. This is a rather interesting analysis, as the original design was based only on prescriptive rules for earthquake resistance, as is the case of many traditional masonry buildings around the world.

4.1.1. FEM model

Figures 20 and 21 show the deformed shapes and the damage level for the four analysis, +X (S-N), –X (N-S), +Y (E-W) and –Y (W-E), representing the two earthquake directions and the left-to-right and right-to-left actions. Damage is measured by the maximum

principal strain, which is associated with the crack width. In the case of the +X direction it is possible to see in Figure 20a the collapse of the South gable, with cracks appearing on the top of the NE and NW edges and on the left side of the North gable (Figure 20b). In the –X direction the SW corner of the building collapses in Figure 20c, and cracks appear in the North façade and interior walls of the Council Chambers (Figure 20d).

In the +Y direction, from Figure 21a there is deformation of the West façade to the outside and there is extensive damage on the gables of the North and South façades, with cracks in the interior walls near the Council Chambers (Figure 21b). In the –Y direction, the top arch on the right of the South façade collapses and the turret in the SE corner is damaged in Figure 21c, and there are cracks in the interior walls near the East façade (Figure 21d).

In the case of the FEM model, several displacement control points were defined in the façades, by default at the top center of the walls, and the corresponding capacity curves were obtained. Then, from all the curves, the one that is considered to best represent the behavior of the building is selected, in each direction. Note that the average displacement was not considered, due to the fact that control points are at different levels and also because some points presented very large displacements due to the collapse of some building parts. Figure 22 shows the capacity curves for all analysis corresponding to maximum load factors of 0.16, 0.13, 0.24 and 0.15 for +X, –X, +Y and –Y loadings respectively. Here, this is the percentage of the weight of the building applied horizontally, or the base shear force in proportion. Therefore, the building can withstand a static horizontal action of 0.13g, being more vulnerable in the –X direction.

A different behavior is identified for the +Y direction, which, from the observation of the evolution of damage and displacement in the computed response, seems to be due to the fact that the transversal walls to the East façade are working as buttresses for the building. These walls are working in elastic range (without significant damage) up to a displacement of

100 mm, allowing to considerably increase the base shear strength, after that the damage in the walls appears with corresponding decreasing of the base shear, see Figure 21a-b. This effect is not observed in the –Y direction, where the transversal walls present early damage, as shown in Figure 21c-d.

The failure mode in the X direction is the collapse of the SW corner of the building, and the roof is not modeled in the simulation. As the roof might provide a certain level of restraint at the top of those walls, another model was prepared using tyings between the nodes of the top left of the South façade and the top right of the North façade. This tries to simulate the existence of a relatively stiff roof in the Council Chamber, with a good connection between roof purlins and walls, or the addition of steel ties between the walls. The new analyses in the X direction provide similar results for each loading sign. In Figure 23 it is shown that a much different behavior of the building is found due to ties in the Council Chamber (refer to Figure 20a-b). The new capacity curve for that direction can be found in Figure 24, when compared with previous analysis, where it is shown that the capacity increase is moderate and virtually extinguishes for larger displacements.

4.1.2. EFM model

Figures 25 to 28 present deformed shapes and damage states corresponding to the analysis in the ±X (S-N) and ±Y (E-W) directions. Note that the deformed shapes are significantly magnified by the value in square brackets, with maximum displacement at the top of the building lower than 0.02 m. In the case of the +X loading, a rotation of the East body of the building is identified in Figure 25a-b with major displacements in the East elevation. In this façade, at the peak strength most elements are plastic by flexure, after which a flexural mechanism of the ground storey occurs with a large drop in the base shear strength.

For the –X loading, see Figure 26, a pronounced in-plane displacement of the wall P8 is initially identified (see also Figure 27a), with subsequent aggravation of the in-plane displacements and damage (mainly flexural) of walls in the East body of the building, e.g. wall P17 in Figure 27b. The low density and insufficient continuity of walls, mainly in the ground storey, represents a possible weakness.

The results of the analyses in the Y direction, shown in Figures 28 and 29, denote the fragility of the South half-façade in the East body (set of walls P10 to P15), with a stiffness much lower than the one of the half-façade in the West side (P7). For this reason, a significant fraction of lateral load is absorbed by the wall P9, which fails early by a first storey flexural mechanism, as shown in Figure 30. The same kind of failure is identified for the wall P22 only at the ultimate state, as in Figure 31a, given the large length of the piers. The stronger wall in this direction is the P5, presenting very low damage and deformation (Figure 31b).

Figure 32 presents the building capacity curves obtained in all directions. The peak base shear is computed respectively for +X, –X, +Y and –Y as 0.27, 0.22, 0.18 and 0.10 of the building weight. The curves for X direction exhibit a higher peak base shear but also a more brittle response. Note that this brittle response is in part due to hypothesis of the model, which considers that a masonry pier is able only to sustain horizontal loads until an ultimate drift. On the other hand, a significant inelastic reserve is identified in Y direction. Note that these results are not directly comparable with the previous FEM model results, as diaphragmatic action is considered for the floors and out-of-plane failure is not considered in the EFM model. Still, both models predict consistently global capacities in the range between 0.10 and 0.25*g* for the four analyses, with the minimum global capacity of the building about 10% of its weight, which is rather low. The results seem to indicate that the use of prescriptive rules at the end of the 19th century in New Zealand for masonry buildings provide a much unsafe result and corroborate the catastrophic damage observed in recent earthquakes.

4.2. Results Corresponding to the Altered Structure through the EFM Model

The studied building was subjected to structural changes by a renovation in 1989, which has been identified on a collection of sketches obtained from the Christchurch City Council. These drawings show that several alterations have been made inside the building with much use of reinforced concrete. Several walls were removed and others were replaced, such as walls P8 and P17 in Figure 33 (refer to Figure 27 for a comparison).

The macro-element model was updated by introducing the main changes in the building structure, with the aim to evaluate the influence of the alterations in the pushover response. From the computed capacity curves in Figure 34, it seems that the influence in the global building response of the intervention made is very low. The peak values of the base shear are about the same, but a slightly improved ductility is observed due to the reinforced concrete elements contribution.

A final analysis was made considering a bidirectional diaphragm for all floors of the building, which can simulate a possible strengthening intervention with adequate tying of the building. This model can also replicate the existing behavior if the previous structural alterations managed to reach this goal, which cannot be confirmed at this stage without a careful inspection of the building from the inside (currently forbidden due to safety reasons). An example of a possible solution to change a unidirectional timber floor to a bidirectional diaphragm floor is presented in Figure 35, by using a multi-plank system with transversal joists.

The results in Figure 36, comparing the unidirectional and bidirectional floors, clearly show a significant improvement of the building response for bidirectional floors, both in terms of base shear and ductility. The minimum capacity of the building (in the +Y direction) is now about 20% of the weight, or 0.2g. The capacity increase for the –Y direction is

dramatic. The assumed box behavior provides a uniform pattern of translational in-plane displacements, as shown in Figure 37 for the +X and –Y loading directions.

5. Seismic Assessment

A significant uncertainty remains about a number of features of the building, such as the floor system, due to modifications to which the building has been subjected in the 1989 renovation and to the fact that access to the building interior is impossible. For this reason, a performance-based seismic assessment including a force verification was preferred, instead of a displacement-based safety assessment that can be very sensitive to non-validated deformation characteristics. Effectively, the obtained results from the modal analysis seems to be unreliable, which large discrepancies in the predictions from the FEM and EFM models. For this reason, the fundamental mode shapes and corresponding periods of the structure were not computed. In opposition to the procedure in the N2 method [Fajfar and Fischinger, 1988], where an equivalent single-degree-of-freedom system is used, in this study the idealized bilinear response of the real building was considered. The inelastic capacity of the building is accounted through a ductility-based behavior factor q, and it was assumed that the building needs to withstand the maximum spectral acceleration (MSA) registered in the February 2011 quake.

Figure 38 compares the capacity curves obtained from the pushover analysis on the FEM and 1D floor EFM models. Note that the results from EFM and FEM are not directly comparable, given that the diaphragmatic action is considered for the floors in the EFM model while out-of-plane failure is considered in the FEM model, and given that the assumed response of masonry piers in the EFM is brittle. Effectively, a discrepancy is observed of the predicted peak strength in the X direction, which is possibly due mostly to absence of floors in the FEM model, and because the floors in the EFM model work mainly in the X direction.

In the Y direction the approximation between the two models is better. The results of both predictions seem to be very conservative, in the sense that the building survived the February 2011 Christchurch quake with a MSA of 1.0*g* (note that the MSA in the New Zealand code NZS 2004 is 0.66*g*). Therefore, it is assumed that the EFM with the 2D floor model is the one better representing the present condition of the building, as the new capacity curves in Figure 39 provide higher strength and ductility.

The subsequent computations are based in the definition of an idealized bilinear representation of the building capacity curves. The idealized bilinear response is computed by defining the initial branch with a secant stiffness *k* for 70% of the maximum base shear in the capacity curve, and the subsequent horizontal plateau is defined by equalizing the energy of the actual and idealized responses until a displacement (d_u) corresponding to a post-peak base shear capacity of 80%. The yield point of the idealized response is defined by the displacement d_y and by the load factor F_y/W, where W is the building weight. The idealized bilinear response of the building corresponding to all loading directions is presented in Figure 39, with the associated parameters from Table 2. A ductility-based behavior factor q_μ is also computed according to Tomaževič [2007] as:

$$q_\mu = \sqrt{2\mu - 1} \tag{1}$$

where μ is the global ductility computed as the ratio between d_u and d_y.

On the other hand, the reference spectrum ordinates S_r can be computed by reducing the MSA measured (1.0*g*) using the behavior factor q_μ, leading to the results given in Table 3. A basic safety factor *SF* can then be computed as the ratio between the normalized base shear strength F_y/W and the reference spectrum ordinate S_r. The computed SF values provide insufficient resistance of the building to survive the 2011 Christchurch quake, being the +Y direction the weakest. The reason of this underestimation is mainly due to the assumed brittle behavior of the masonry elements, which provides a conservative response both in terms of

base shear and ductility. Tomaževič [2007] suggests, based in shaking table tests, an over-strength of at least 30%, as a result of underestimation for material strength. If this over-strength is accounted in the computation of an increased safety factor *ISF*, a higher seismic resistance is observed for the building, already close to the unit value and justifying why the same survived the earthquake, even if with considerable damage.

6. Conclusions

Powerful tools have been developed and are now widely disseminated for the seismic assessment of complex buildings, particularly those made with masonry, a material that possesses a very low tensile strength and for which the usage of linear elasticity is unreasonable. In this work, a study on the seismic behavior of the "Old Municipal Chambers" building in Christchurch, New Zealand, which was significantly damaged by recent earthquakes, was made using two modeling approaches, a finite element method (FEM) model and an equivalent frame method (EFM) model, which were analyzed through pushover loading. Both techniques are easily available today, even if the first method requires usually large preparation and computation times and large number of degrees-of-freedom, in opposition to the second method that is relatively expedite and uses a very low number of degrees-of-freedom.

Additionally, the FEM model considers both in-plane and out-of-plane damage of the structural elements, and is capable of replicating local damage, e.g. around the "Industry" statue and on the chimney in the SW corner of the building. On the hand, the EFM model considers only the in-plane response of the walls by using a macroscopic simulation of the flexural and shear responses, which allows only capturing the global behavior of the building. The EFM model requires therefore that the building is properly tied by adequate diaphragms, which is not always the case in traditional masonry buildings. In general, it can be stated, that

the FEM model presents the most flexible representation of the building response, while the EFM models presents a complementary, expedite, first approach. In the present case, the modeling efforts and the validation of the results are partly compromised by the fact that the building has external shoring and access to its interior is forbidden due to safety reasons.

Although the maximum values on the capacity curves for the FEM and EFM approaches are different, the general behavior of the building is captured and the fragile and most robust areas of the building have been well identified. This information will be used in the current strengthening design of the building. Both models consistently provide largely insufficient capacity of the structure, which seems incorrect as the building survived the 2010-2011 Christchurch earthquakes, heavily damaged.

Therefore, a final EFM model with bidirectional diaphragmatic floor providing "box behavior" to the building was prepared. This model gives a significant increase on the building general capacity, doubling it, with considerable ductility. In this case, a performance-based assessment including a force verification quantitatively indicates almost sufficient earthquake resistance of the building to survive the February 2011 Christchurch quake with a MSA of 1.0*g*, as observed. The better-than-expected performance of the building when subjected to the high MSA in this earthquake was also due to the short duration of the event.

Acknowledgements

The authors gratefully acknowledge Professor Jason Ingham and his research group at University of Auckland for providing experimental data in Christchurch and their recommendations on materials properties to be expected. The two first authors acknowledge the financial support from the Portuguese Foundation for Science and Technology (FCT) through PhD grants SFRH/BD/41221/2007 and SFRH/BD/45436/2008.

References

Anthoine, A., Magenes, G. and Magonette, G. [1995] "Shear-compression testing and analysis of brick masonry walls," *Proceedings of the 10th European Conference on Earthquake Engineering*, Vienna, pp. 1657–1662.

ATC [2005] *Improvements of Nonlinear Static Seismic Analysis Procedures, FEMA 440,* American Technical Council, Washington.

Bradley, B. [2011] "Ground motions observed at recording stations in the 13th June events (1:01pm and 2:20pm)," Preliminary Summary Report, Bradley Seismic Ltd., Canterbury.

Calderini, C. and Lagomarsino, S. [2008] "A continuum model for in-plane anisotropic inelastic behavior of masonry," *ASCE Journal of Structural Engineering* **134**(2), 209–220.

CEN [2004] *Eurocode 8, Design of Structures for Earthquake Resistance – Part 1: General Rules, Seismic Actions and Rules for Buildings, EN 1998-1:2004*, European Committee for Normalization, Brussels.

Fajfar, P. and Fischinger, M. [1988] “N2 – a method for nonlinear seismic analysis of regular buildings,” *Proceedings of the 9th World Conference on Earthquake Engineering*, Vol. 5, Tokyo-Kyoto, pp. 111–116.

Fusco, E., Penna, A., Prota, A., Galasco, A. and Manfredi, G. [2008] “Seismic assessment of historical natural stone masonry buildings through non-linear analysis,” *Proceedings of the 14th World Conference on Earthquake Engineering*, Beijing, CD-ROM.

Galasco, A., Lagomarsino, S., Penna, A. and Resemini, S. [2004] “Non-linear analysis of masonry structures,” *Proceedings of the 13th World Conference on Earthquake Engineering*, Vancouver, Paper No. 843.

Galasco, A., Lagomarsino, S., Penna, A., and Cattari, S. [2009] TreMuri Program: Seismic Analyser of 3D Masonry Buildings, Version 1.7.34, User Guide, University of Genoa.

Gambarotta, L. and Lagomarsino, S. [1996] “On the dynamic response of masonry panels,” in *Proceedings of the Italian Conference “La meccanica delle murature tra teoria e progetto”*, ed. L. Gambarotta, Messina, pp. 451–462 (in Italian).

Lignola, G. P. and Cosenza, E. [2009] “Historical interventions on the Treasure of St. Gennaro’s Chapel in Naples, Italy: Numerical analyses and damage assessment,” *Proceedings of the International Conference PROHITECH 09 on Protection of Historical Buildings*, Rome; Taylor & Francis Group, London, pp. 161–167.

Lourenço, P. B. [2000] “Anisotropic softening model for masonry plates and shells,” *ASCE Journal of Structural Engineering* **126**(9), 1008–1016.

Lourenço, P. B., Krakowiak, K. J., Fernandes, F. M. and Ramos, L. F. [2007] “Failure analysis of Monastery of Jerónimos, Lisbon: How to learn from sophisticated numerical models,” *Engineering Failure Analysis* **14**(2), 280–300.

Lourenço, P. B. and Roque, J. A. [2006] “Simplified indexes for the seismic vulnerability of ancient masonry buildings,” *Construction and Building Materials* **20**(4), 200–208.

Lourenço, P. B. [2009] “Recent advances in masonry structures: Micromodelling and homogenization,” in *Multiscale Modeling in Solid Mechanics: Computational Approaches*, eds. U. Galvanetto and M. H. Ferri Aliabadi, Imperial College Press, pp. 251–294.

Lourenço, P. B., Mendes, N., Ramos, L. F. and Oliveira, D. V. [2011] “Analysis of masonry structures without box behavior,” *International Journal of Architectural Heritage* **5**(4–5), 369–382.

Lumantarna, R. [2012] “Material Characterisation of New Zealand’s Clay Brick Unreinforced Masonry Buildings,” Ph.D. thesis, The University of Auckland, New Zealand, available from https://researchspace.auckland.ac.nz/handle/2292/18879.

Mann, W. and Müller, H. [1982] “Failure of shear-stressed masonry – An enlarged theory, tests and application to shear walls,” *Proceedings of the British Ceramic Society*, Vol. 30, Stoke-on-Trent, pp. 223–235.

Marques, R. and Lourenço, P. B. [2011] "Possibilities and comparison of structural component models for the seismic assessment of modern unreinforced masonry buildings," *Computers and Structures* **89**(21–22), 2079–2091.

Milani, G., Lourenço, P. B. and Tralli, A. [2007] "3D Homogenized limit analysis of masonry buildings under horizontal loads," *Engineering Structures* **29**(11), 3134–3148.

NTC [2008] *Norme Tecniche per le Costruzioni (Technical Standards for Construction)*, Ministero Infrastrutture e Trasporti, Rome (in Italian).

NZS [2004] *Structural Design Actions – Part 5: Earthquake Actions – New Zealand, NZS 1170.5*, Standards New Zealand, Wellington.

Peña, F., Prieto, F., Lourenço, P. B., Campos Costa, A. and Lemos, J. V. [2007] "On the dynamics of rocking motion of single rigid–block structures," *Earthquake Engineering and Structural Dynamics* **36**(15), 2383–2399.

Ramos, L. F. and Lourenço, P. B. [2004] "Advanced numerical analysis of historical centers: A case study in Lisbon," *Engineering Structures* **26**(9), 1295–1310.

Rots, J. G. [1988] "Computational Modeling of Concrete Fracture," Ph.D. thesis, Delft University of Technology, The Netherlands.

Russell, A. P., Mahmood, H. and Ingham, J. M. [2007] “Assessment of the material properties of New Zealand’s unreinforced masonry building stock,” in *Proceedings of the 3rd International Conference on Structural Engineering, Mechanics and Computation*, ed. A. Zingoni, Cape Town, South Africa; Millpress, The Netherlands, pp. 1623–1628.

Russell, A. P. and Ingham, J. M. [2010] “Prevalence of New Zealand’s unreinforced masonry buildings,” *Bulletin of the New Zealand Society for Earthquake Engineering* **43**(3), 182–200.

Selby, R. G. and Vecchio, F. J. [1993] “Three-dimensional constitutive relations for reinforced concrete,” Technical Report 93-02, Dept. of Civil Eng., Univ. of Toronto, Canada.

S.T.A. DATA [2010] 3Muri, “Software per muratura,” Version 4.0.3, User Manual, S.T.A. DATA S.r.l., Turin, URL: http://www.stadata.com.

TNO [2009] DIANA, DIsplacement method ANAlyser, Release 9.4, User’s Manual, TNO DIANA BV, The Netherlands.

Tomaževič, M. [1978] “The computer program POR,” Report ZRMK, Ljubljana (in Slovenian).

Tomaževič, M. [2007] “Damage as a measure for earthquake-resistant design of masonry structures: Slovenian experience,” *Canadian Journal of Civil Engineering* **34**, 1403–1412.

Turnšek, V. and Čačovič, F. [1970] “Some experimental results on the strength of brick masonry walls,” *Proceedings of the 2nd International Brick Masonry Conference*, Stoke-on-Trent, pp. 149–156.

van der Pluijm, R. [1999] “Out of Plane Bending of Masonry: Behaviour and Strength,” Ph.D. thesis, Eindhoven University of Technology, The Netherlands.

Walters, A. and Parker, W. [2011] “Post-earthquake structural shoring: Old Municipal Chambers, Christchurch,” Report Issue 3, Opus International Consultants Limited, Christchurch Office.

TABLE 1 Properties of the masonry

f_m	*Compressive strength*	5.0 MPa
τ_0	*Pure shear strength*	0.1 MPa
w	*Weight*	18.0 kN/m^3
E	*Elastic modulus*	2,500 MPa
G	*Shear modulus*	417 MPa
δ_f	*Flexural limit drift*	0.006
δ_s	*Shear limit drift*	0.004
f_t	*Tensile strength*	0.15 MPa
G_c	*Compressive fracture energy*	8 N/mm
G_f^I	*Mode I-fracture energy*	0.012 N/mm

TABLE 2 Parameters of the idealized bilinear responses

	d_y (mm)	k (kN/m)	F_y/W	d_u (mm)	μ	q_μ
$+X$	2.67	930311	0.294	14.80	5.54	3.18
$-X$	3.01	789091	0.282	14.10	4.68	2.89
$+Y$	1.78	898841	0.190	12.40	6.97	3.60
$-Y$	3.09	837500	0.307	23.13	7.49	3.74

TABLE 3 Computation of reference spectrum ordinates and safety factors

	S_r (g)	F_y/W (g)	*SF*	*ISF*
$+X$	0.315	0.294	0.93	1.21
$-X$	0.346	0.282	0.82	1.07
$+Y$	0.278	0.190	0.68	0.88
$-Y$	0.268	0.307	1.15	1.50

Figure Captions

FIGURE 1 Early photo of the Old Municipal Chambers building [ca. 1890, Image from Christchurch City Libraries, File Reference: CCL PhotoCD 3, IMG0034. Source: Archive 334, p. 87].

FIGURE 2 Structural plans of the (a) ground and (b) first storeys (original configuration).

FIGURE 3 Horizontal view of East elevation and section from South (original drawings by Samuel Hurst Seager, ca. 1886).

FIGURE 4 Details of the building: (a) "Industry" statue, (b) window's frames and (c) ground floor support.

FIGURE 5 Response spectra recorded near the studied building for several seismic events, in terms of accelerations and displacements [Bradley, 2011].

FIGURE 6 Views of the building (a) before [Photo by Phillip Capper under Creative Commons, at http://en.wikipedia.org/wiki/File:OxfordTerraceChristchurch13June2008.jpg] and (b) after the 2010-2011 Christchurch earthquakes.

FIGURE 7 Indoor views of the Council Chamber: (a) North [ca. 1921, Image from Christchurch City Libraries, File Reference: CCL PhotoCD 12, IMG0032. Source: The Imperial album of New Zealand scenery, p. 229] and (b) South [Photo by Robert Cutts under Creative Commons, at http://commons.wikimedia.org/wiki/File:Former_Council_Chamber,_Christchurch,_NZ.jpg].

FIGURE 8 Main damage on the North façade.

FIGURE 9 Main damage on the East façade.

FIGURE 10 Main damage on the South façade.

FIGURE 11 Main damage on the West façade.

FIGURE 12 FEM mesh of the building and model detail of the East gable.

FIGURE 13 Masonry modeling: (a) quadrilateral 8 nodes shell element and (b) stress-strain diagrams for the masonry behavior in tension and compression [TNO, 2009].

FIGURE 14 Kinematic model for the macro-element [Gambarotta and Lagomarsino, 1996].

FIGURE 15 Criteria for the macro-element strength to (a) bending-rocking and (b) diagonal shear.

FIGURE 16 Wall discretization and tridimensional assemblage of a building [adapted from Galasco *et al.*, 2004].

FIGURE 17 Modeling of the building: 3D macro-element model and floor model plan.

FIGURE 18 Examples of two views of the EFM model.

FIGURE 19 Modeling of the gable in the East façade (dashed lines denote the force flow).

FIGURE 20 Deformed shape and damage for +X: (a) collapse of South gable and (b) damage without South gable, and –X: (c) collapse of SW corner and (d) damage without SW corner.

FIGURE 21 Deformed shape and damage for +Y: (a) wide damage of the Council Chambers and (b) damage without the Council Chambers, and –Y: (c) collapse of the top arch in South façade and (d) damage without SE corner.

FIGURE 22 Capacity curves from the FEM analysis.

FIGURE 23 Deformed shape and damage state for the +X analysis with the tyings option.

FIGURE 24 Comparison of capacity curves without and with tyings.

FIGURE 25 Plan deformed shape for the +X analysis related (a) to the peak base shear [x50] and (b) to the ultimate state [x20], and damaged state of (c) East (18.3mm aver. def. at 7.7m) and (d) West (5.2mm aver. def. at 7.7m) elevations relating to peak base shear [x20].

FIGURE 26 Plan deformed shape for the –X analysis corresponding (a) to the peak base shear [x50] and (b) to the ultimate state [x20].

FIGURE 27 Damaged state, due to the –X loading, of the walls (a) P8 (just after the peak base shear, for 23mm wall top displacement) and (b) P17 (for 42mm wall top displacement) [x20].

FIGURE 28 Plan deformed shape for the +Y analysis related (a) to the peak base shear [x50] and (b) to the ultimate state [x20], and damaged state of (c) South (23.1mm aver. def. at 7.7m) [x20] and (d) North (2.1mm aver. def. at 7.7m) [x50] elevations relating to peak base shear.

FIGURE 29 Plan deformed shape for the –Y analysis related (a) to the peak base shear [x50] and (b) to the ultimate state [x20].

FIGURE 30 Flexural mechanisms of the first storey for the wall P9 due to the (a) +Y and (b) –Y loadings just after the peak base shear [x10].

FIGURE 31 Damaged state of the walls (a) P22 due to the +Y loading and (b) P5 due to the –Y loading at the ultimate state [x20].

FIGURE 32 Capacity curves of the building corresponding to all the analysis.

FIGURE 33 Damaged state, due to the –X loading, of the remodeled walls (a) P8 and (b) P17 for similar loading levels to those in Figure 27 (r.c. elements in gray; // flexural damage) [x20].

FIGURE 34 Capacity curves obtained for the original and changed building structures.

FIGURE 35 Possible solution to provide a bidirectional diaphragm floor with a multi-plank system.

FIGURE 36 Capacity curves obtained for the altered building considering 1D and 2D floors.

FIGURE 37 Plan deformed shape for the (a) +X and (b) –Y analysis corresponding to the peak base shear [x50].

FIGURE 38 Comparison of capacity curves obtained for the FEM and 1D floor EFM models.

FIGURE 39 Idealized bilinear responses of the building for the EFM with 2D floor model.

FIGURE 1 Early photo of the Old Municipal Chambers building [ca. 1890, Image from Christchurch City Libraries, File Reference: CCL PhotoCD 3, IMG0034. Source: Archive 334, p. 87].

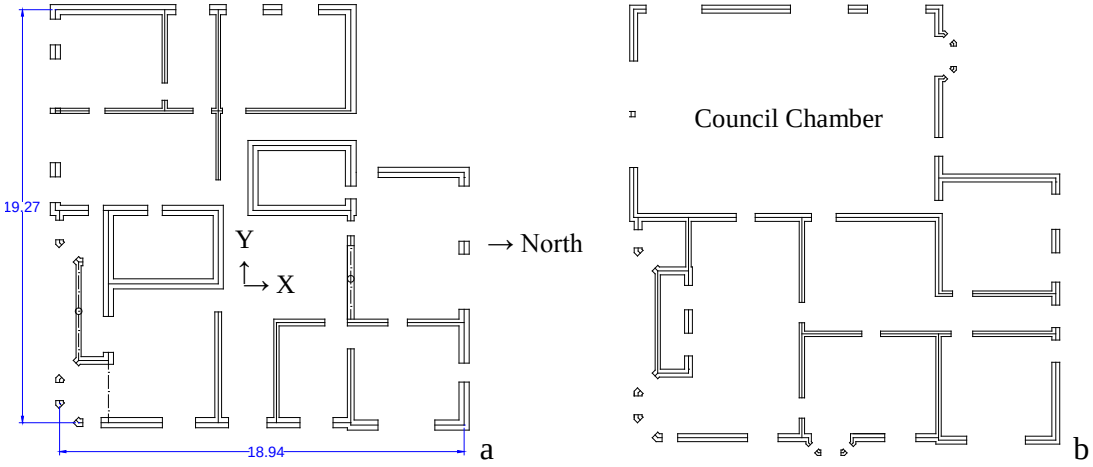

FIGURE 2 Structural plans of the (a) ground and (b) first storeys (original configuration).

FIGURE 3 Horizontal view of East elevation and section from South (original drawings by Samuel Hurst Seager, ca. 1886).


a

b

c

FIGURE 4 Details of the building: (a) “Industry” statue, (b) window’s frames and (c) ground floor support.

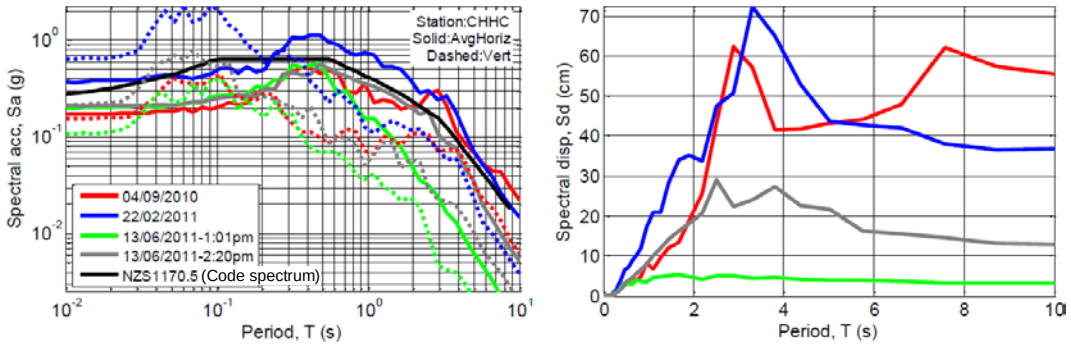

FIGURE 5 Response spectra recorded near the studied building for several seismic events, in terms of accelerations and displacements [Bradley, 2011].


a

b

FIGURE 6 Views of the building (a) before [Photo by Phillip Capper under Creative Commons, at http://en.wikipedia.org/wiki/File:OxfordTerraceChristchurch13June2008.jpg] and (b) after the 2010-2011 Christchurch earthquakes.

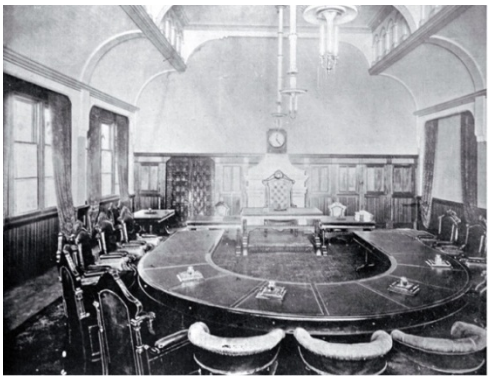
a

b

FIGURE 7 Indoor views of the Council Chamber: (a) North [ca. 1921, Image from Christchurch City Libraries, File Reference: CCL PhotoCD 12, IMG0032. Source: The Imperial album of New Zealand scenery, p. 229] and (b) South [Photo by Robert Cutts under Creative Commons, at http://commons.wikimedia.org/wiki/File:Former_Council_Chamber,_Christchurch,_NZ.jpg].

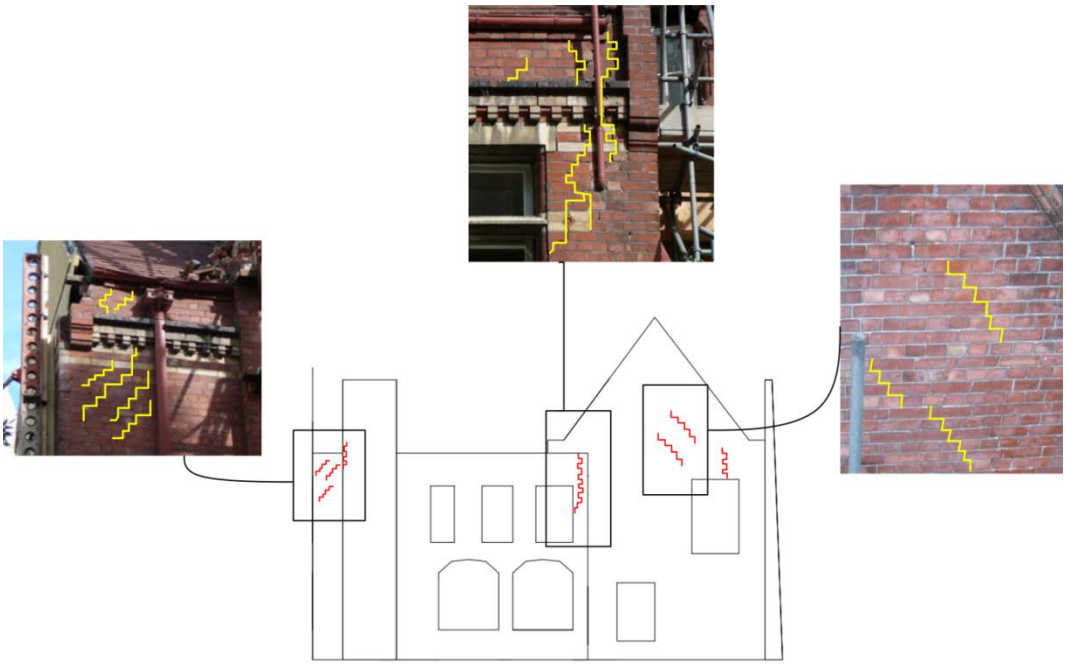

FIGURE 8 Main damage on the North façade.

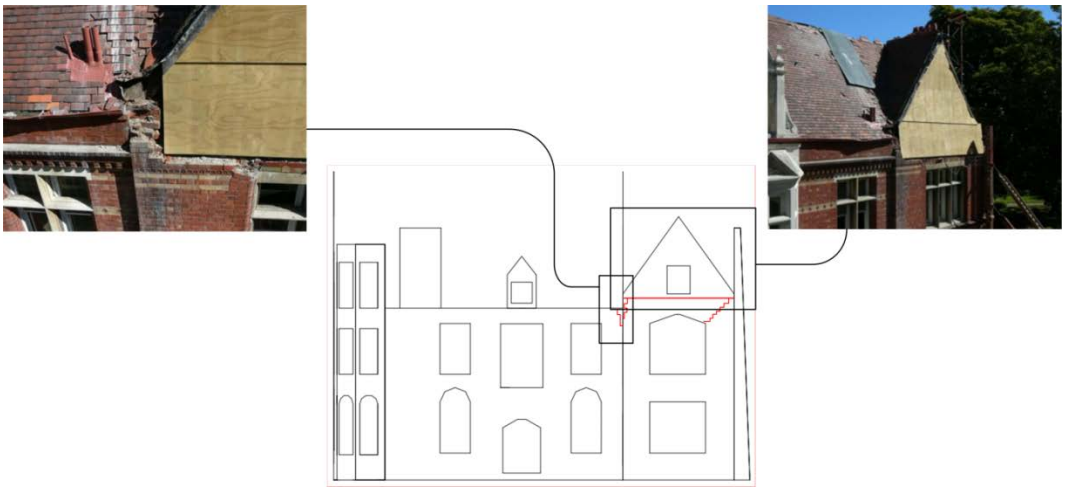

FIGURE 9 Main damage on the East façade.

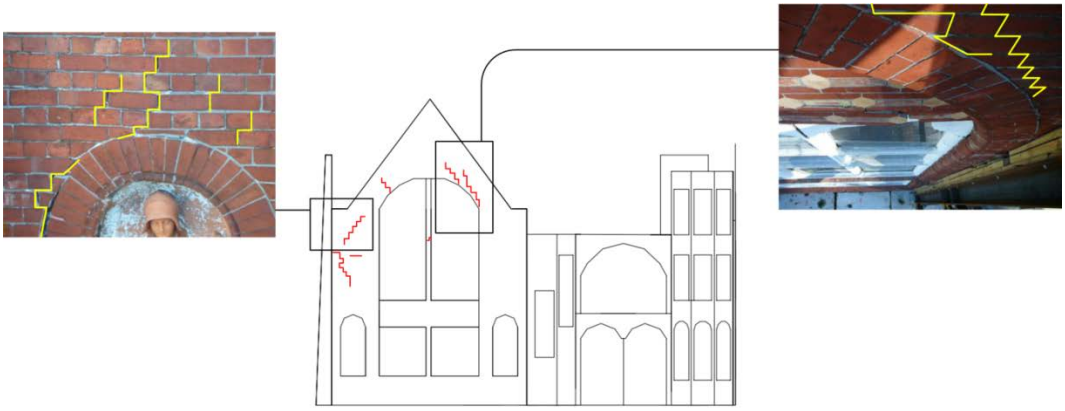

FIGURE 10 Main damage on the South façade.

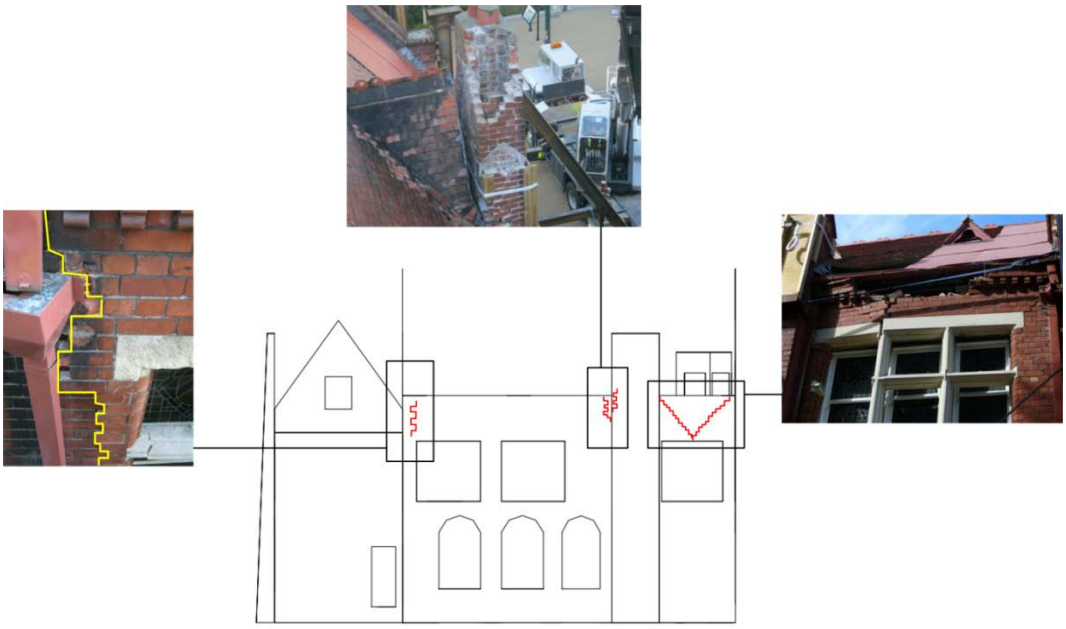

FIGURE 11 Main damage on the West façade.

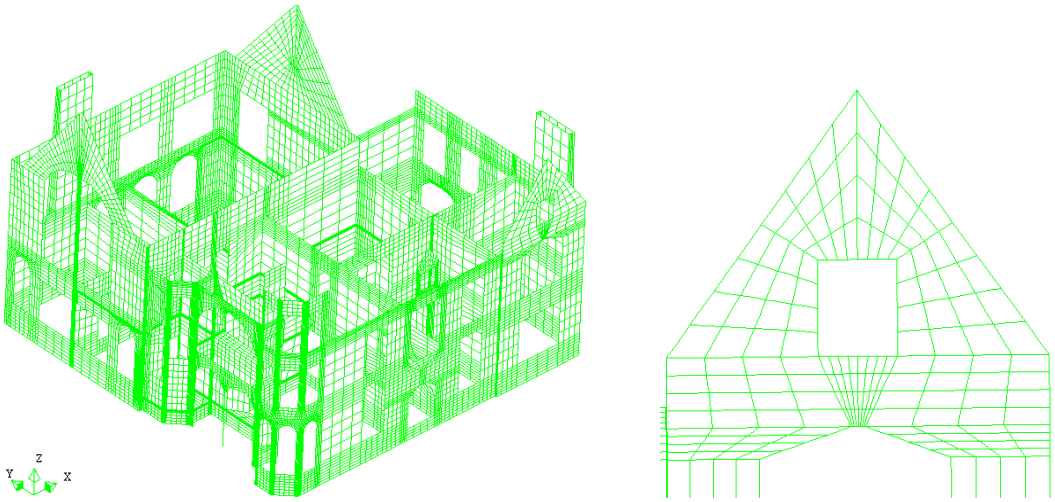

FIGURE 12 FEM mesh of the building and model detail of the East gable.

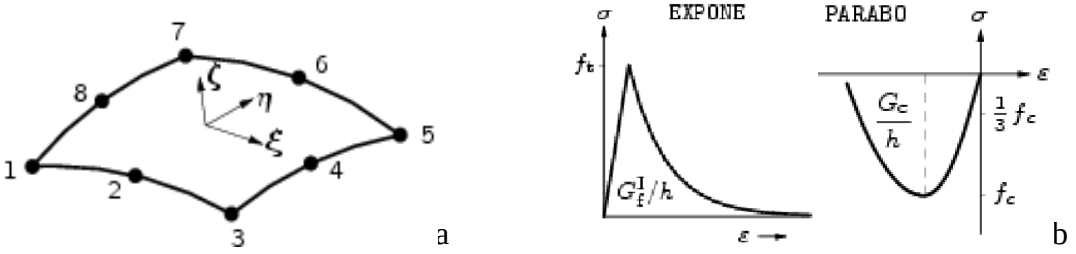

FIGURE 13 Masonry modeling: (a) quadrilateral 8 nodes shell element and (b) stress-strain diagrams for the masonry behavior in tension and compression [TNO, 2009].

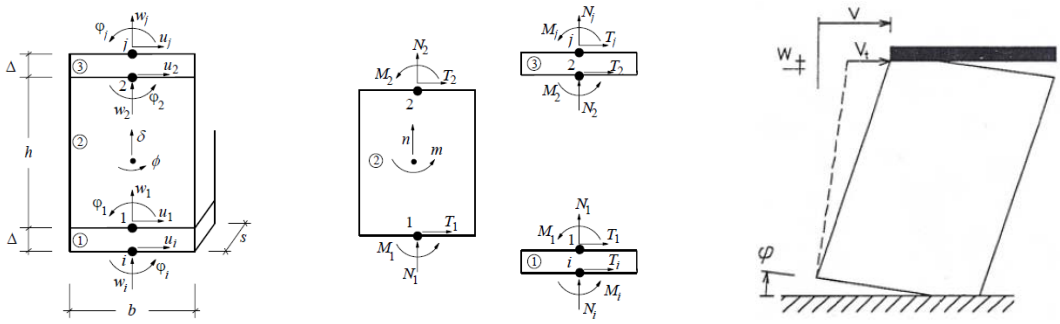

FIGURE 14 Kinematic model for the macro-element [Gambarotta and Lagomarsino, 1996].

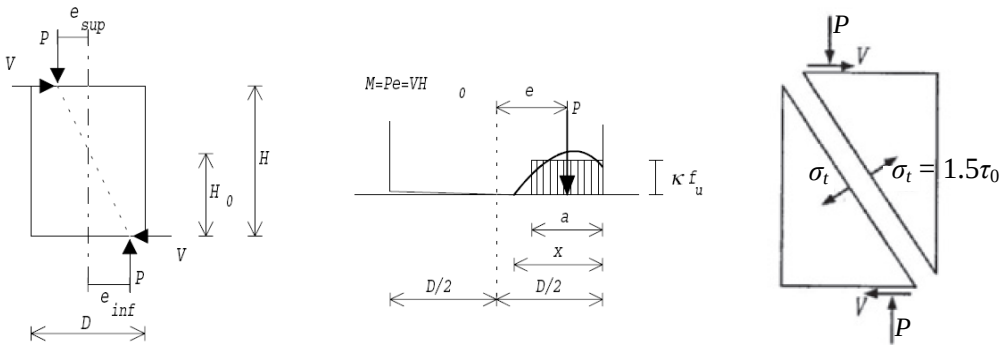

$$M_u = \frac{D^2 t.p}{2}\left(1-\frac{p}{K f_u}\right)$$

$$V_u = Dt\frac{1.5\tau_0}{b}\sqrt{1+\frac{p}{1.5\tau_0}}$$

(a) (b)

FIGURE 15 Criteria for the macro-element strength to (a) bending-rocking and (b) diagonal shear.

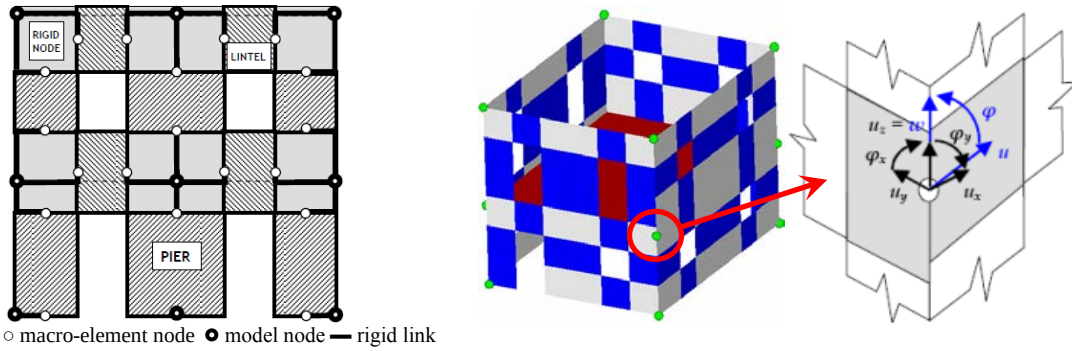

FIGURE 16 Wall discretization and tridimensional assemblage of a building [adapted from Galasco *et al.*, 2004].

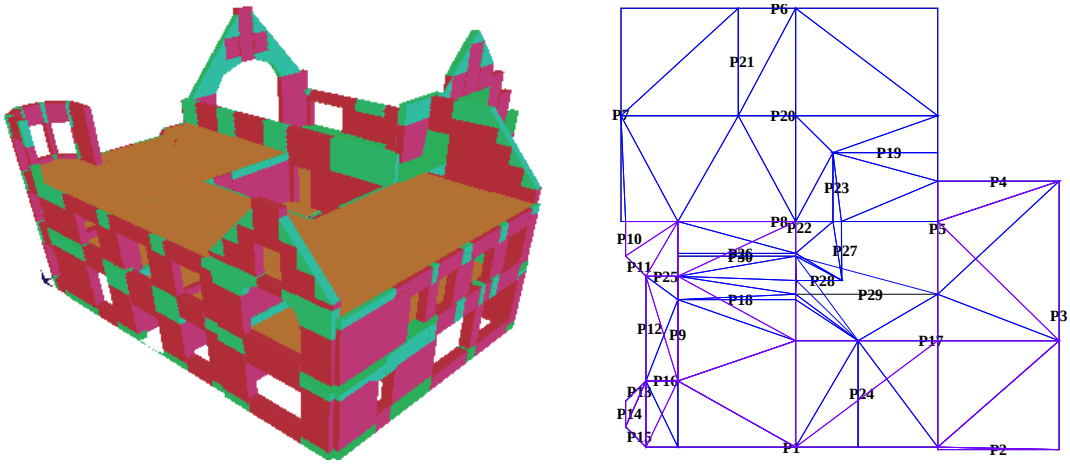

FIGURE 17 Modeling of the building: 3D macro-element model and floor model plan.

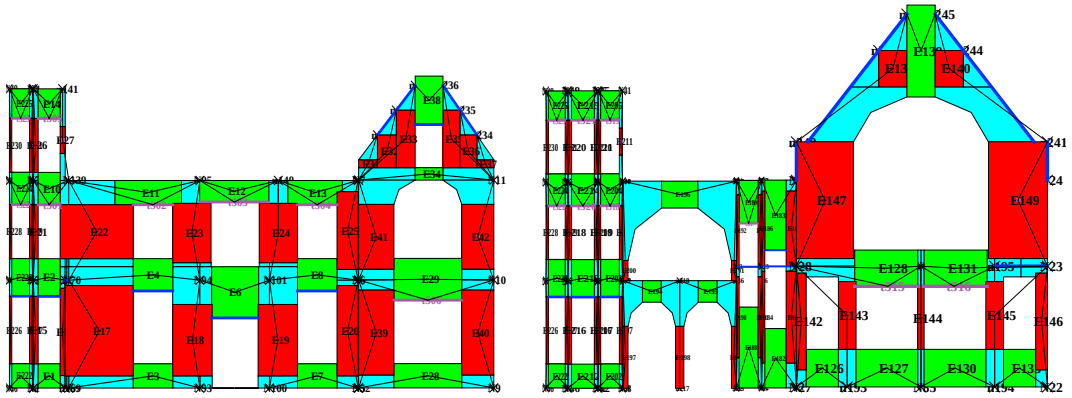

East South (view from inside)

FIGURE 18 Examples of two views of the EFM model.

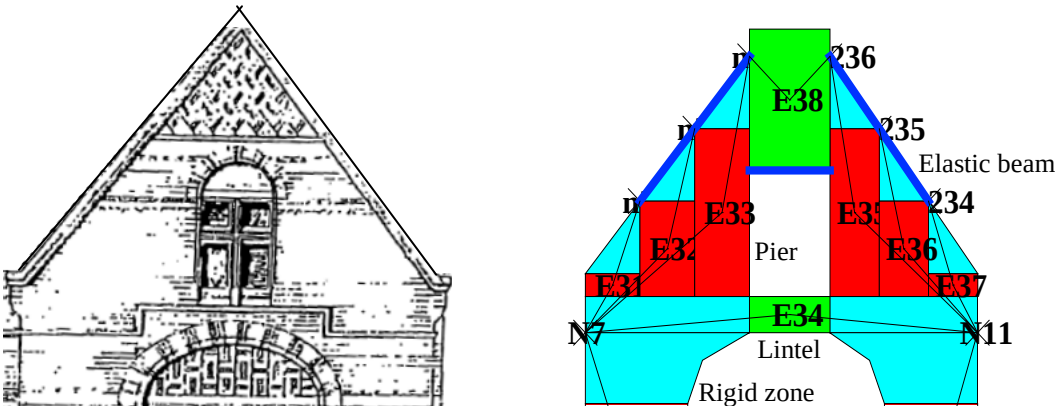

FIGURE 19 Modeling of the gable in the East façade (dashed lines denote the force flow).

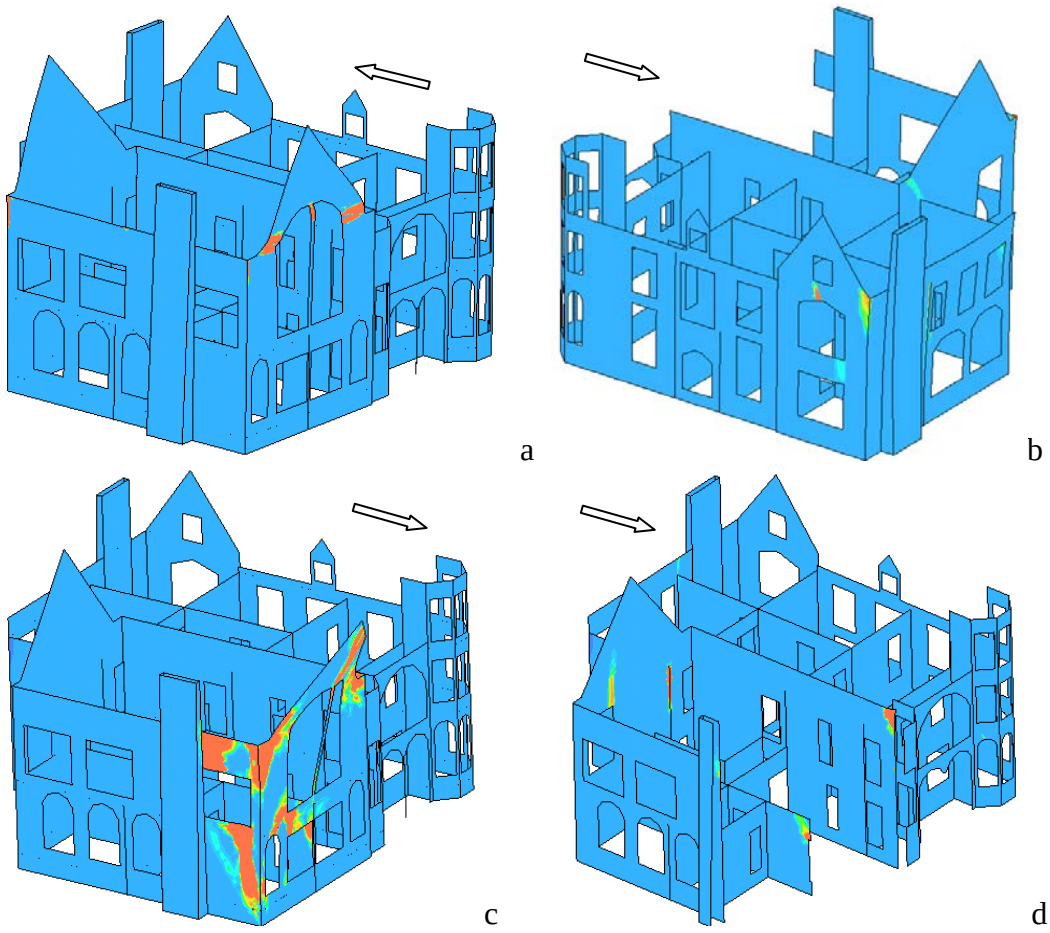

FIGURE 20 Deformed shape and damage for +X: (a) collapse of South gable and (b) damage without South gable, and –X: (c) collapse of SW corner and (d) damage without SW corner.

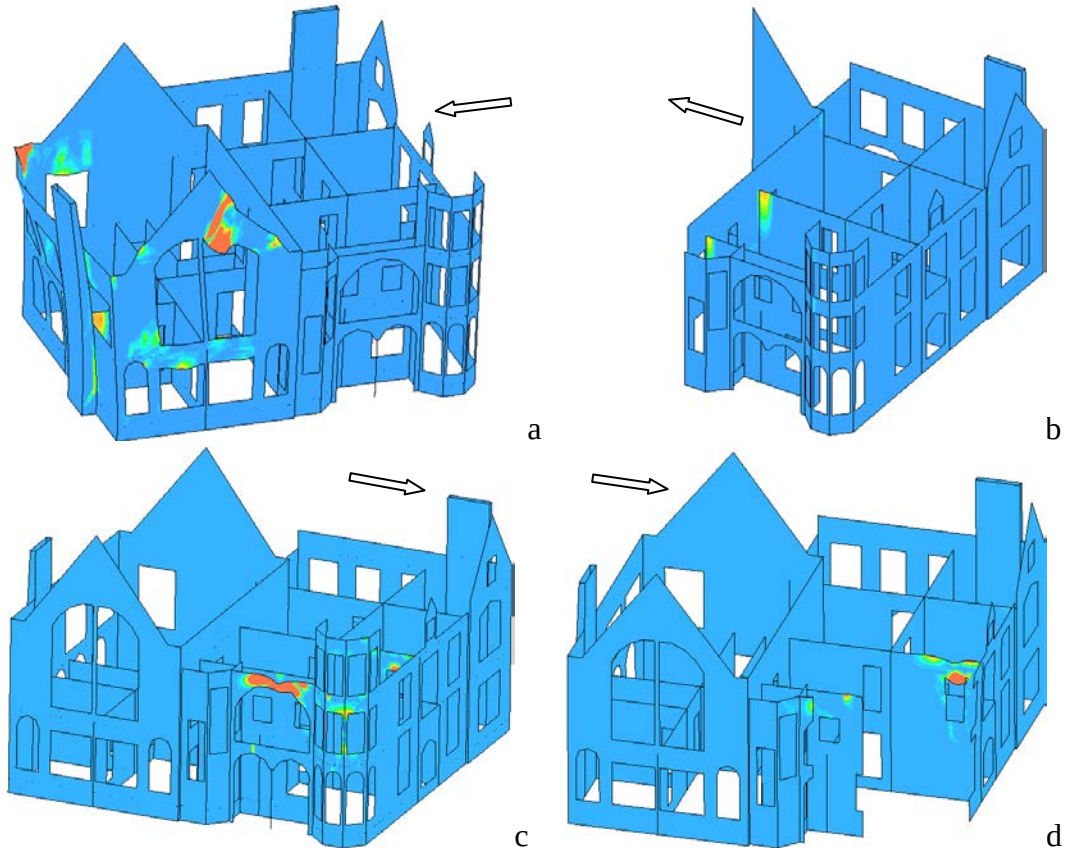

FIGURE 21 Deformed shape and damage for +Y: (a) wide damage of the Council Chambers and (b) damage without the Council Chambers, and –Y: (c) collapse of the top arch in South façade and (d) damage without SE corner.

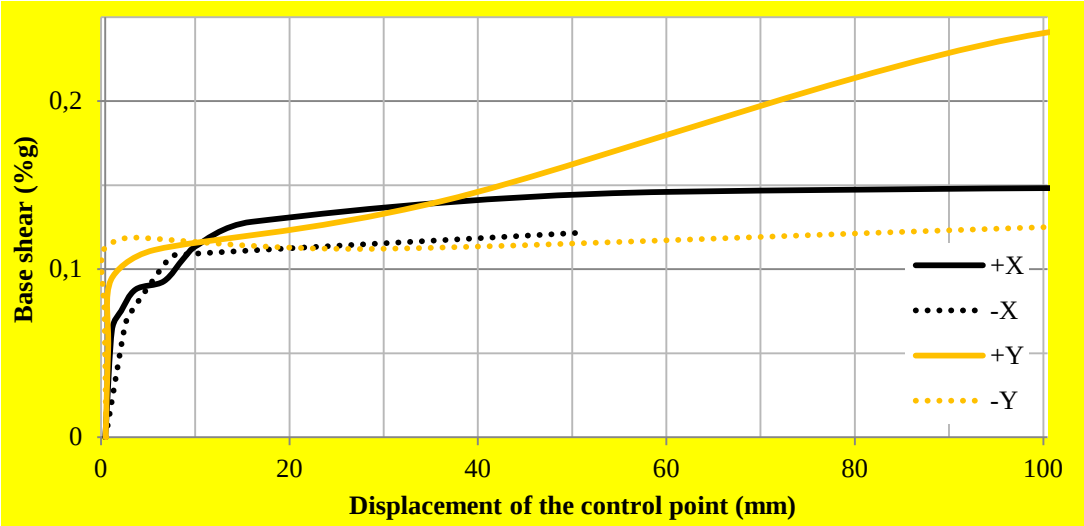

FIGURE 22 Capacity curves from the FEM analysis.

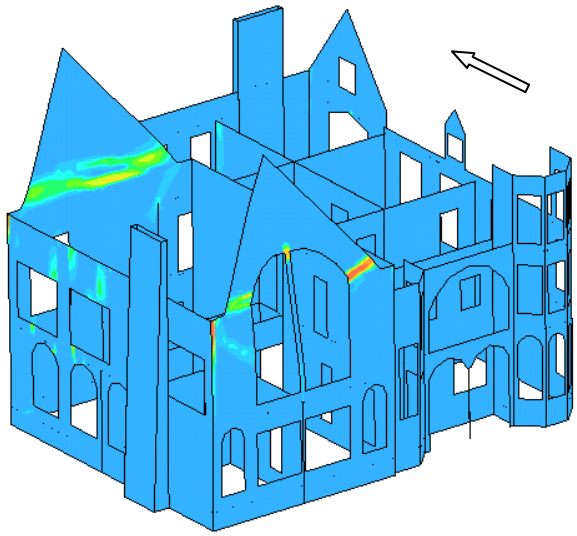

FIGURE 23 Deformed shape and damage state for the +X analysis with the tyings option.

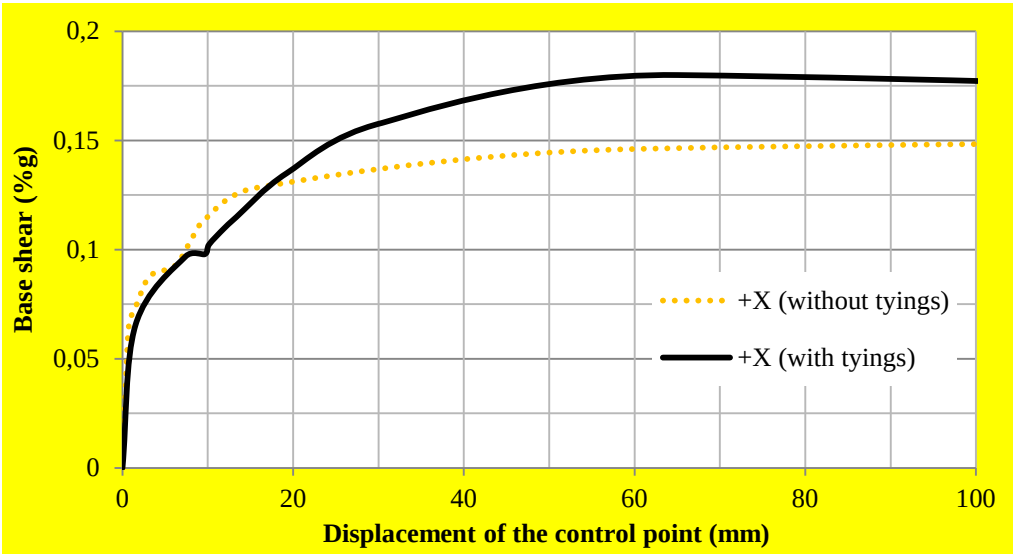

FIGURE 24 Comparison of capacity curves without and with tyings.

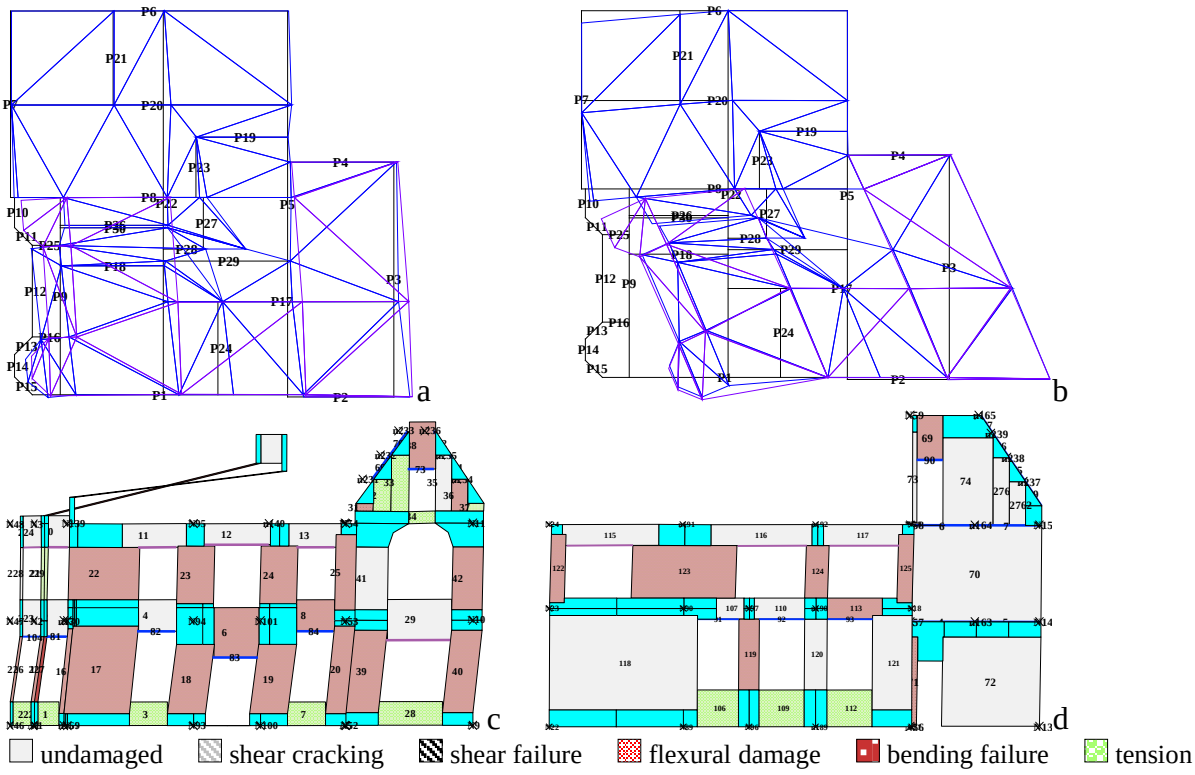

FIGURE 25 Plan deformed shape for the +X analysis related (a) to the peak base shear [x50] and (b) to the ultimate state [x20], and damaged state of (c) East (18.3mm aver. def. at 7.7m) and (d) West (5.2mm aver. def. at 7.7m) elevations relating to peak base shear [x20].

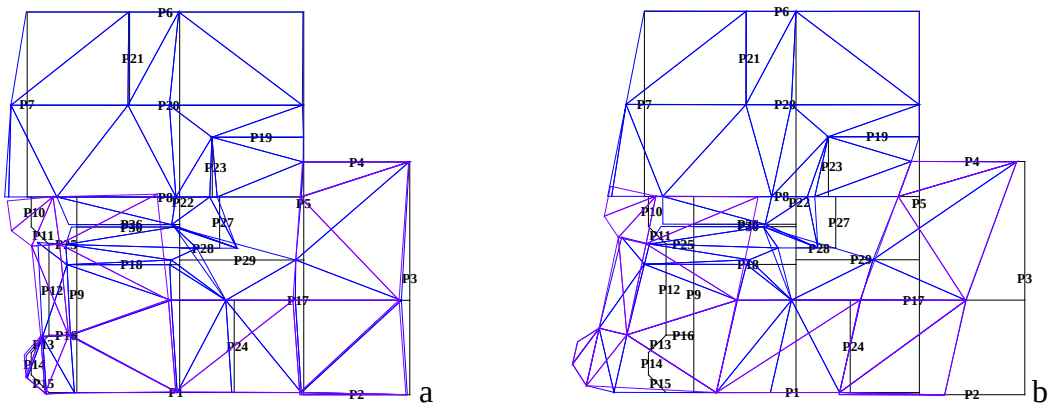

FIGURE 26 Plan deformed shape for the –X analysis corresponding (a) to the peak base shear [x50] and (b) to the ultimate state [x20].

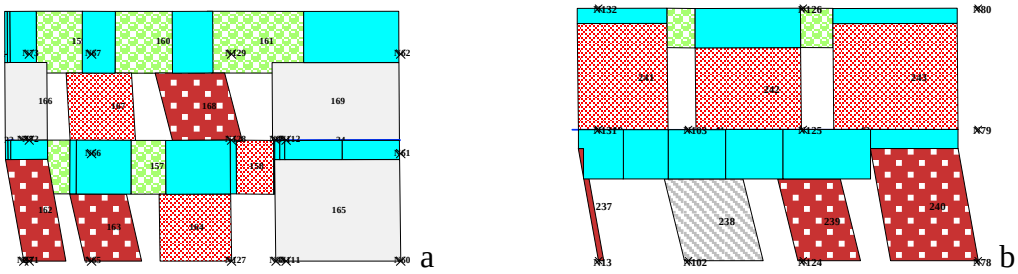

FIGURE 27 Damaged state, due to the –X loading, of the walls (a) P8 (just after the peak base shear, for 23mm wall top displacement) and (b) P17 (for 42mm wall top displacement) [x20].

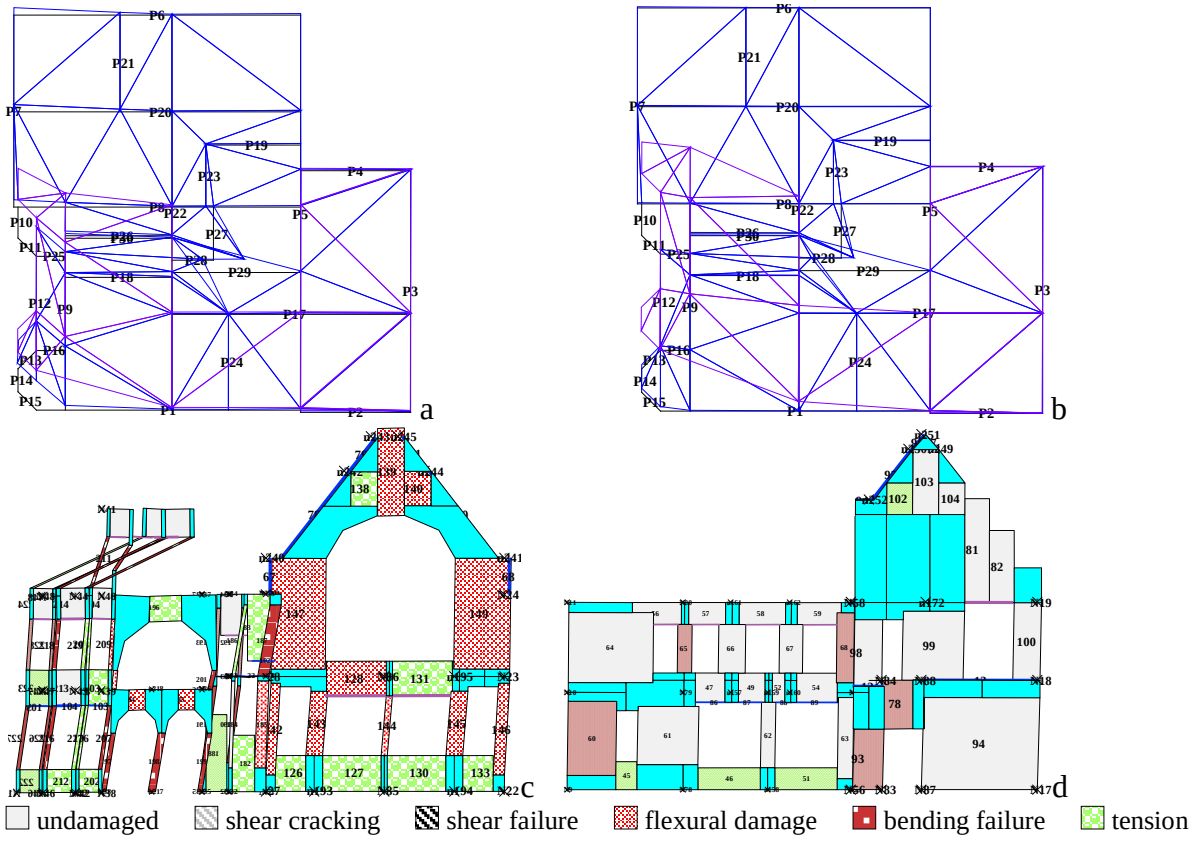

FIGURE 28 Plan deformed shape for the +Y analysis related (a) to the peak base shear [x50] and (b) to the ultimate state [x20], and damaged state of (c) South (23.1mm aver. def. at 7.7m) [x20] and (d) North (2.1mm aver. def. at 7.7m) [x50] elevations relating to peak base shear.

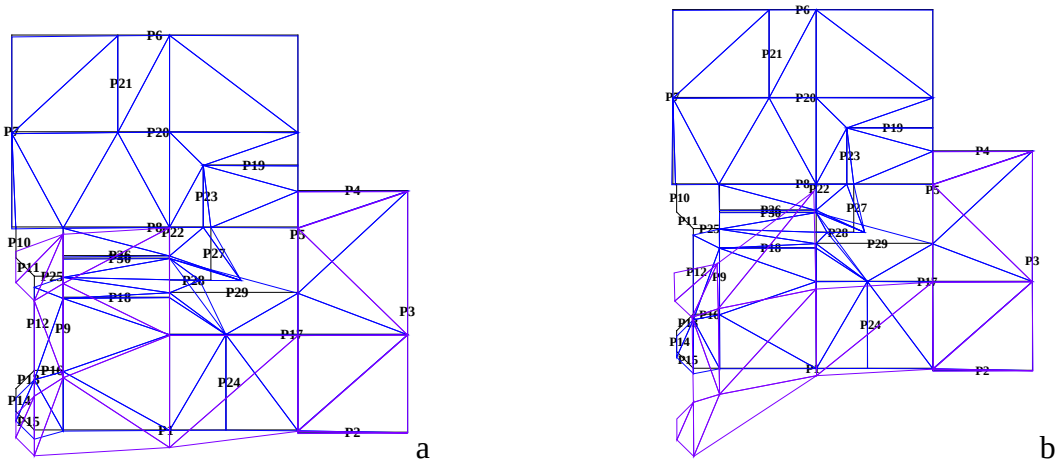

FIGURE 29 Plan deformed shape for the –Y analysis related (a) to the peak base shear [x50] and (b) to the ultimate state [x20].

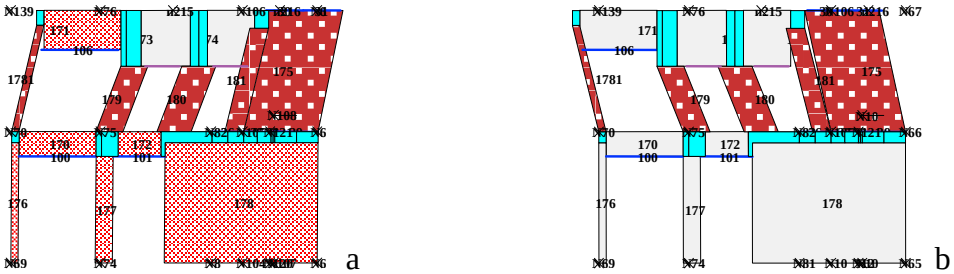

FIGURE 30 Flexural mechanisms of the first storey for the wall P9 due to the (a) +Y and (b) –Y loadings just after the peak base shear [x10].

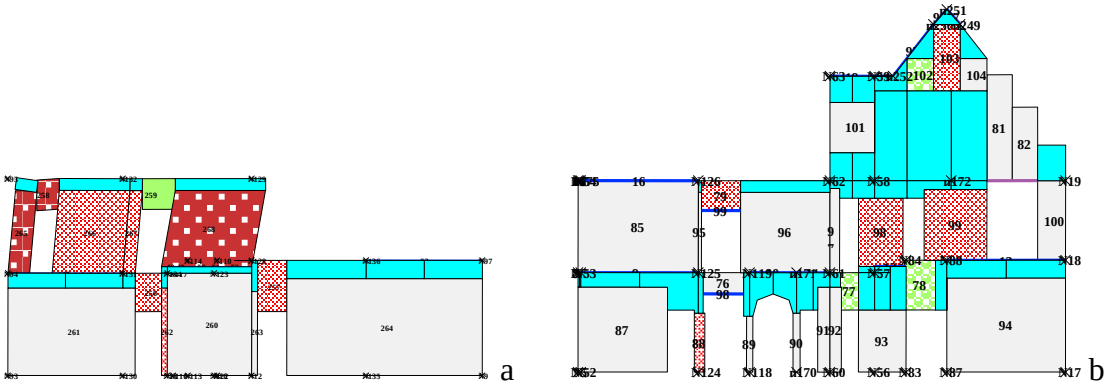

FIGURE 31 Damaged state of the walls (a) P22 due to the +Y loading and (b) P5 due to the –Y loading at the ultimate state [x20].

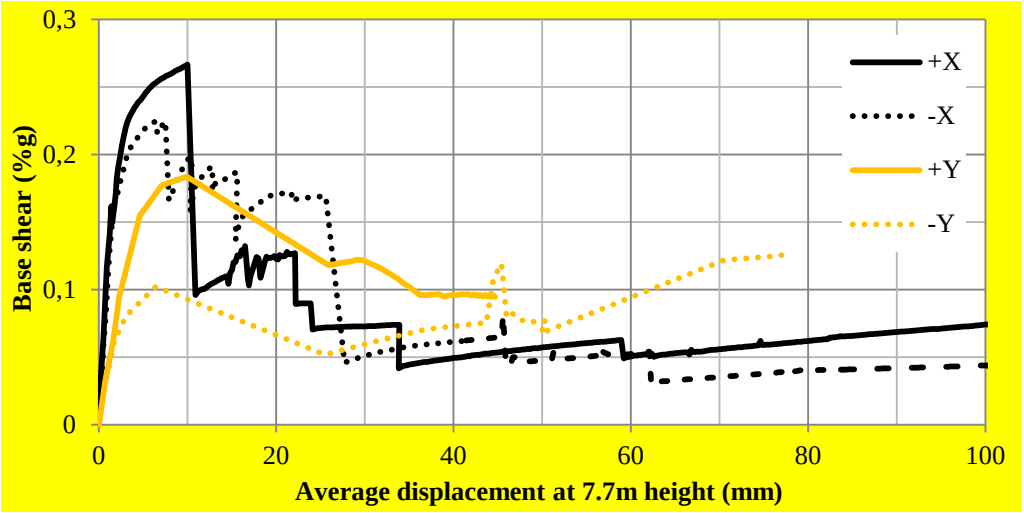

FIGURE 32 Capacity curves of the building corresponding to all the analysis.

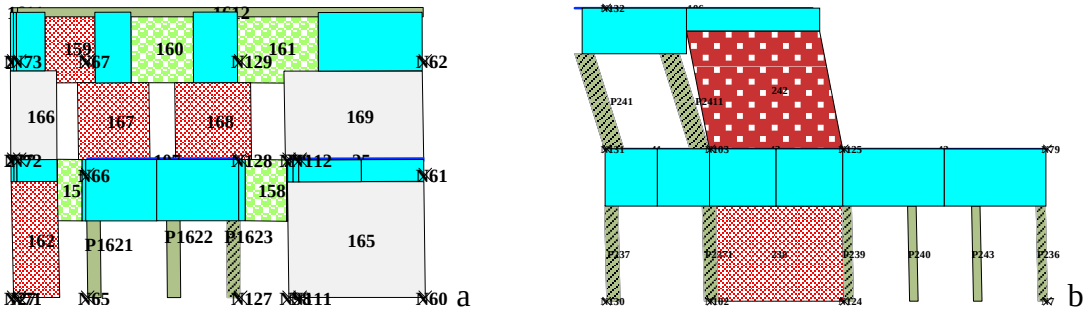

FIGURE 33 Damaged state, due to the –X loading, of the remodeled walls (a) P8 and (b) P17 for similar loading levels to those in Figure 27 (r.c. elements in gray; // flexural damage) [x20].

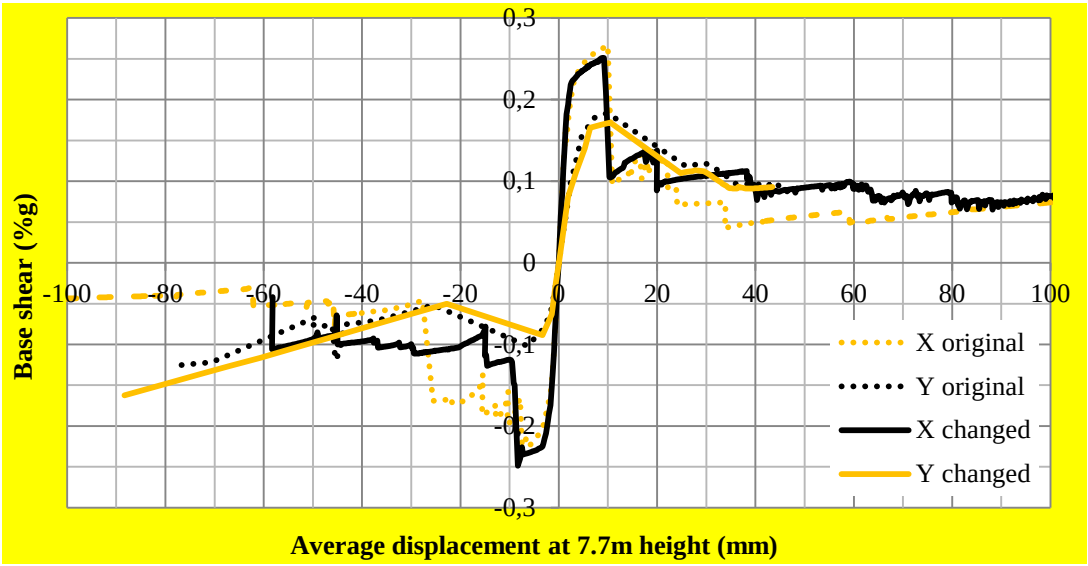

FIGURE 34 Capacity curves obtained for the original and changed building structures.

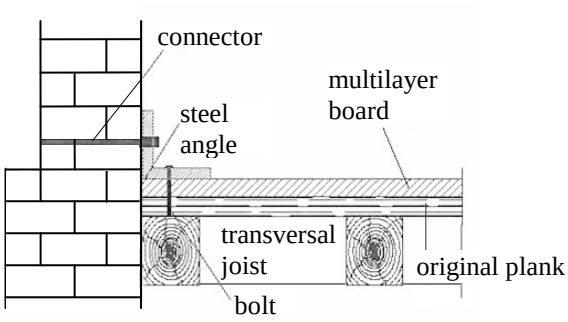

FIGURE 35 Possible solution to provide a bidirectional diaphragm floor with a multi-plank system.

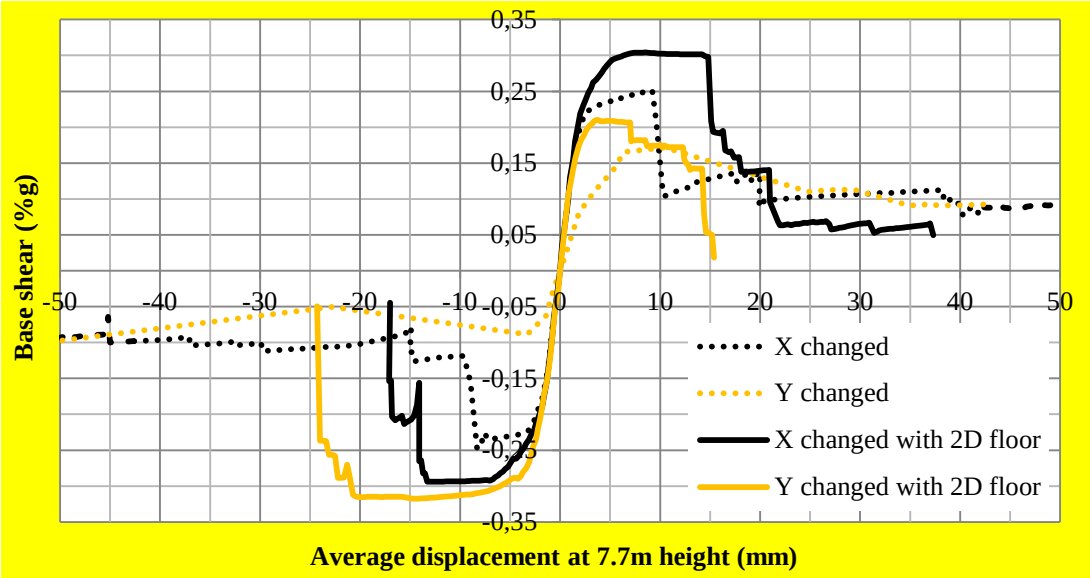

FIGURE 36 Capacity curves obtained for the altered building considering 1D and 2D floors.

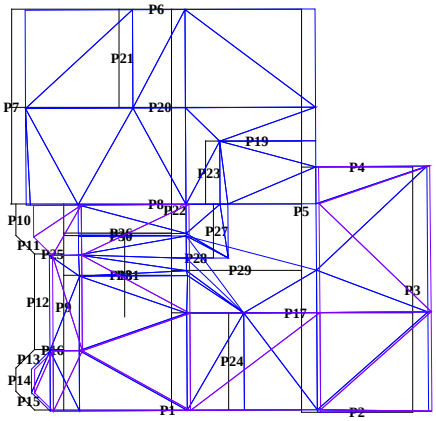

a

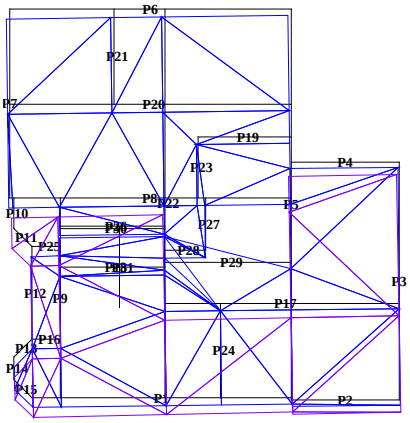

b

FIGURE 37 Plan deformed shape for the (a) +X and (b) –Y analysis corresponding to the peak base shear [x50].

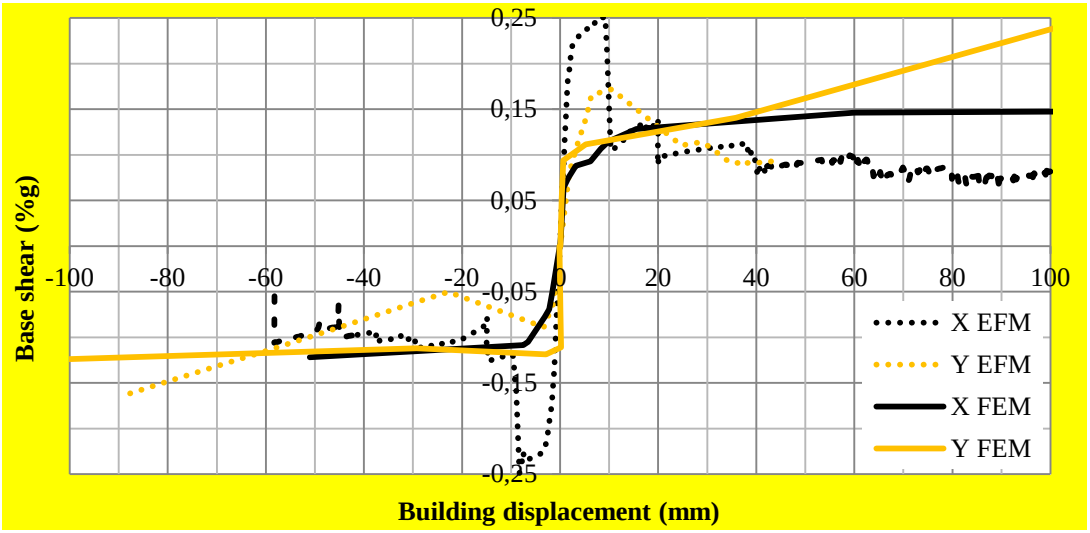

FIGURE 38 Comparison of capacity curves obtained for the FEM and 1D floor EFM models.

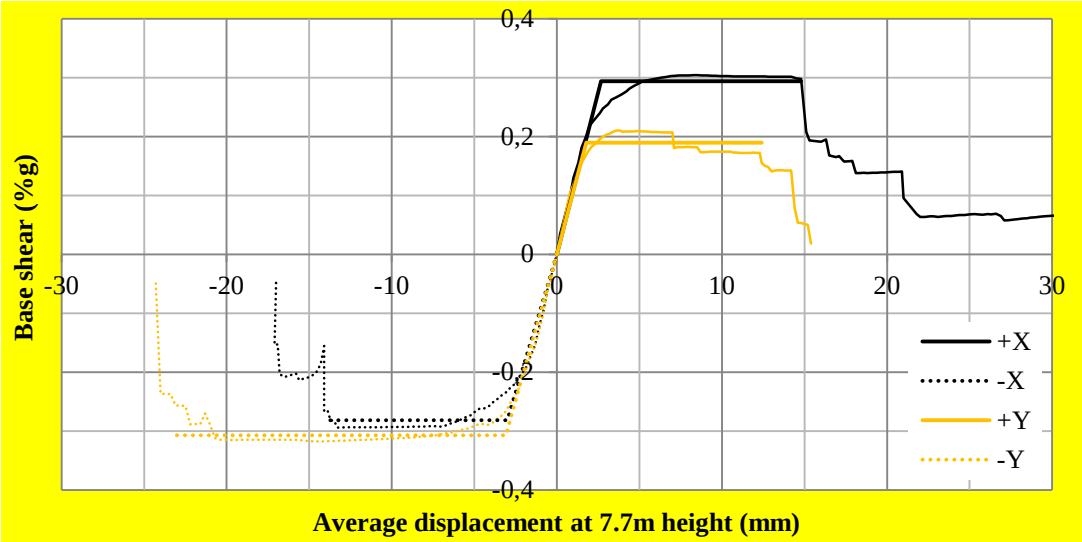

FIGURE 39 Idealized bilinear responses of the building for the EFM with 2D floor model.